UDC 551.574.1:551.576.11

Numerical Simulation of Precipitation Development in Supercooled Cumuli—Part II

WILLIAM R. COTTON—*Experimental Meteorology Laboratory, NOAA, Coral Gables, Fla.*

ABSTRACT—A numerical model of supercooled cumuli is developed and discussed. Water substance in the model is idealized to be partitioned into the five phase components; namely, water vapor, liquid cloud water, liquid rainwater, frozen rainwater, and ice crystals. Continuity equations are developed that predict the distribution of water substance among the five phase components. The cloud dynamic framework consists of a simple one-dimensional Lagrangian model that includes the effects of entrainment. The model is able to operate either as a steady-state model or as a spherical vortex model.

The results of two case study experiments illustrated that the principle action of ice particles nucleated on sublimation nuclei, or by the freezing of cloud droplets in cumulus clouds containing moderate to heavy amounts of supercooled rainwater, is to promote the freezing of supercooled rainwater. On the other hand, clouds containing small amounts of supercooled rainwater are dynamically insensitive to moderate concentrations of ice crystals. In such clouds, extensive riming and vapor deposition growth of crystals in concentrations of several thousand per liter are required before they make significant contributions to the dynamic structure of the cloud.

Finally, it was found that the warm-cloud precipitation process can either invigorate or retard the dynamic behavior of a supercooled cloud, depending upon the height and magnitude of the precipitation process.

1. INTRODUCTION

It was demonstrated by Cotton (1972) that the formulation of a reasonable simulation of precipitation development in "warm" cumulus clouds is a particularly difficult problem. However, the supercooled cumulus cloud is further complicated not only by the presence of a broad spectrum of liquid droplets but also by the nucleation and growth of various forms of unrimed, rimed, and aggregated solid hydrometeors.

It is considered here that nucleation of ice particles occurs on, or at the expense of, one of the two partitions of liquid water. For example, if nucleation takes place either by direct activation of sublimation nuclei or by the freezing of cloud droplets, the subsequent crystal formed is said to have been nucleated at the expense of the liquid cloud water partition. On the other hand, the nucleation or freezing of rainwater is considered to be at the expense of the rainwater partition. This will be discussed in further detail in the following sections.

2. RAINWATER FREEZING

Two models of rainwater freezing are considered here. The first model is the heterogeneous freezing of rainwater via the containment of an active freezing nucleus. The second is the freezing of rainwater by the collection of ice crystals nucleated at the expense of liquid cloud water. Additional freezing processes not considered are the freezing by surface collection of nuclei and freezing through mechanical disturbances such as liquid–liquid drop collisions, raindrop breakup, and shock waves. The latter processes are not sufficiently well defined quantitatively to be included in this cloud model.

a. Heterogeneous Freezing of Rainwater

The freezing model derived here is based on the concepts of supercooled drop freezing developed from laboratory experiments. As a first approximation, we consider that the stochastic nature of freezing, as implied by the laboratory experiments of Vali and Stansbury (1966), is a second-order effect. According to the development of Langham and Mason (1958), given a random distribution of nuclei through a bulk water sample, the probability that a drop will freeze is then a function of the concentration of active nuclei per unit volume of water. In particular, they specified the cumulative concentration of nuclei per unit volume of water active at a given supercooling, T_s, as

$$K(T_s)=B_s e^{a_s T_s} \tag{1}$$

where a_s and B_s are experimentally determined constants. (The symbols used in this paper are defined in table 1.)

Based on the Poisson probability of a droplet containing at least one nucleus active at a given supercooling, the cumulative fraction of frozen drops of diameter $D\pm\delta D/2$ is formulated as

$$\frac{N(D,T_s)}{N(D)}=1-\exp\left[\frac{-\pi D^3}{6}K(T_s)\right]. \tag{2}$$

Before one can apply eq (2) to natural clouds, he must be satisfied with the validity of the assumption that nuclei are randomly dispersed throughout a net unit volume or mass of liquid water in actual clouds. There is, unfortunately, a significant difference between a well-mixed laboratory sample of water divided into drops of a given size and the processes of incorporation of aerosol into cloud droplets and raindroplets.

TABLE 1.—*Definitions of symbols*

A_k, B_k	coefficients in eq (39)
A_i'	crystal geometric accretion cross-section
a	length of basal plane axis of crystal
a_s, B_s	coefficients in eq (1)
C	crystal capacitance
C_D	drag coefficient of a crystal or precipitation particle
c	length of prism axis of crystal
c_p	specific heat at constant pressure
D	diameter of precipitation particle
$\overline{D}$	average particle diameter
D_v	diffusivity of water vapor in air
D_w	diameter of precipitation particle suspended by updraft
D_{min}	diameter of smallest frozen raindrop considered
E	collection efficiency employed in eq (41)
$E(D\|C)$	collection efficiency between raindrops of diameter D and cloud droplets
$E(D\|I)_L$	collection efficiency calculated with the Langmuir formula
E_a, E_{HP}	collection efficiencies employed in eq (42)
e	functions defined in table 3
e_s	saturation vapor pressure
F_D	aerodynamic drag force on a crystal
$f(T)$	concentration of ice crystals nucleated over the temperature range $T\pm dT/2$
$f(\mathrm{Re})$	ventilation function
g	acceleration of gravity
K_D	ratio of crystal cross-section to solid cylinder cross-section
K_P, K_N, K_{HP}	crystal aspect ratios defined in table 3
$K(T_s)$	cumulative concentration of freezing nuclei at a given T_s
K_t	molecular thermal conductivity
L_c	latent heat of condensation
LWC	liquid water content
L_f	latent heat of fusion
L_s	latent heat of sublimation
M	rainwater density or liquid water content
$M(D)$	water content of precipitation particles of diameter $D\pm\delta D/2$
M_F	frozen rainwater density or water content
$M_F(>D_w)$	water content of frozen particles greater than D_w
$M_H(>D_w)$	rainwater content greater than D_w
m	cloud water density or water content
m_d	molecular weight of water vapor
N_0	intercept coefficient in eq (18) or the Marshall-Palmer generating function
N_T	total concentration of precipitation particles
$N(D)$	concentration of raindrops of diameter $D\pm\delta D/2$
$N(J)$	cumulative concentration of ice crystals or ice nuclei in class J
$n(J)$	concentration of ice crystals or ice nuclei in class J
$n_e(J)$	concentration of ice nuclei in class J in cloud environment
p	cloud and environment pressure
Q_c	mixing ratio of cloud water
$Q_c(\mathrm{min})$	cloud glaciation threshold
Q_D	rate of molecular diffusion of heat away from a crystal
Q_F	mixing ratio of frozen rainwater
Q_H	mixing ratio of rainwater
Q_I	mixing ratio of ice crystals
Q_s	total mixing ratio of condensed water substance
Q_T	total mixing ratio of water substance
q_e	water vapor mixing ratio of cloud environment
q_s	saturation mixing ratio with respect to water
q_{si}	saturation mixing ratio with respect to ice
q_v	water vapor mixing ratio of cloud
R	cloud radius
R_a	gas constant of air
Re	Reynolds number
S	cloud saturation ratio
T	cloud temperature
T_e	temperature of cloud environment
T_r	surface temperature of crystal
T_s	degree of supercooling of cloud
$T_s(I)$	median temperature of crystal class I
T_v'	perturbation in virtual temperature
T_{vc}, T_{ve}	virtual temperatures of cloud and environment
t	time
u	lateral entrainment velocity
u_0	air velocity relative to an ice crystal
V	volume of precipitation particle
$V_D, V(D)$	fall velocity of supercooled or frozen raindrop
V_I	mean terminal velocity of crystals in class I
V_i, V_T	terminal velocity of an individual ice crystal
$V(I\|_a)$	collection kernel between crystals and cloud droplets
w	cloud updraft velocity
$X(D)$	mass of hydrometeor of diameter D
x_i	mass of an individual ice crystal
$\dot{x}_R$	rate of crystal growth by riming
z	vertical distance
α_a	specific volume of air
α_r	specific volume of reference state
β_s, N_s	coefficients in eq (83)
δ_i	density of ice
δ_i	mean density of frozen precipitation
δ_r	density of rimed ice deposit
δ_s	density of ice formed by vapor deposition
ϵ	ratio of the density of water vapor to air
η	function defined in eq (30)
λ	slope parameter in Marshall-Palmer generating function and eq (19)
μ	entrainment rate
μ_a	molecular kinematic viscosity of air
ξ_1, ξ_2	functions defined in eq (16) and (17)
ρ_a	density of cloudy air
ρ_e	density of cloud environment
ρ_l	density of water
ρ_w	vapor density some distance away from ice crystal
$\rho_w(r)$	vapor density at surface of ice crystal

TABLE 1.—*Concluded*

For convenience, we make the assumption that freezing nuclei are randomly distributed throughout the total rainwater density. Thus, given an estimate of the cumulative spectrum of nuclei active at a given supercooling, eq (2) can then be used to predict the cumulative fraction of droplets of a given diameter that are frozen. The cumulative water content of drops of diameter $D\pm\delta D/2$ that are frozen is then

$$M(D, T_s)_F = X(D)N(D, T_s)_F. \tag{3}$$

If the rainwater is again size distributed in a Marshall-Palmer (1948) distribution, the rainwater content frozen when a population of raindrops is cooled by an amount ΔT_s will be

$$M(\Delta T_s)_F = \frac{\pi\rho_l N_0}{6}\left[\int_0^\infty D^3 e^{-\frac{\pi D^3}{6}K(T_{s1})} e^{-\lambda D} dD - \int_0^\infty D^3 e^{-\frac{\pi D^3}{6}K(T_{s2})} e^{-\lambda D} dD\right] \tag{4}$$

or

$$M(\Delta T_s)_F = \frac{\pi\rho_l N_0}{6}\int_0^\infty D^3 e^{-\lambda D}\left[e^{-\frac{\pi D^3}{6}K(T_{s1})} - e^{-\frac{\pi D^3}{6}K(T_{s2})}\right] dD. \tag{5}$$

Equation (5) is integrated numerically.

In actual cloud experiments, one might find a climatological spectrum of nuclei, $K(T_s)$, from in-cloud rainwater samples. Surface rainwater samples would be of dubious value because of the sweep-out of aersol as they fall from cloud base to the surface. As a control nuclei spectrum, we use the spectrum determined from doubly distilled water by de Pena et al. (1962). The coefficients in eq (1) are thus defined to be $B_s = 1.67\times10^{-5}$ and $a_s = 0.8$. The predicted cumulative fraction of rainwater content frozen for the control nuclei spectrum is plotted in figure 1 for different values of λ corresponding to water contents of 2.0, 1.5, 1.0, 0.5, and 0.25 g·m^{-3}.

b. Freezing by Collection of Ice Crystals

Change in rainwater content. To discuss the freezing of rainwater by collection of ice crystals, one must summarize the essential features of the distribution of ice crystals described in further detail in section 10. There, a 21-element, discrete spectral distribution of ice crystals is described. The concentration of ice crystals nucleated is

478-887 O - 72 - 2

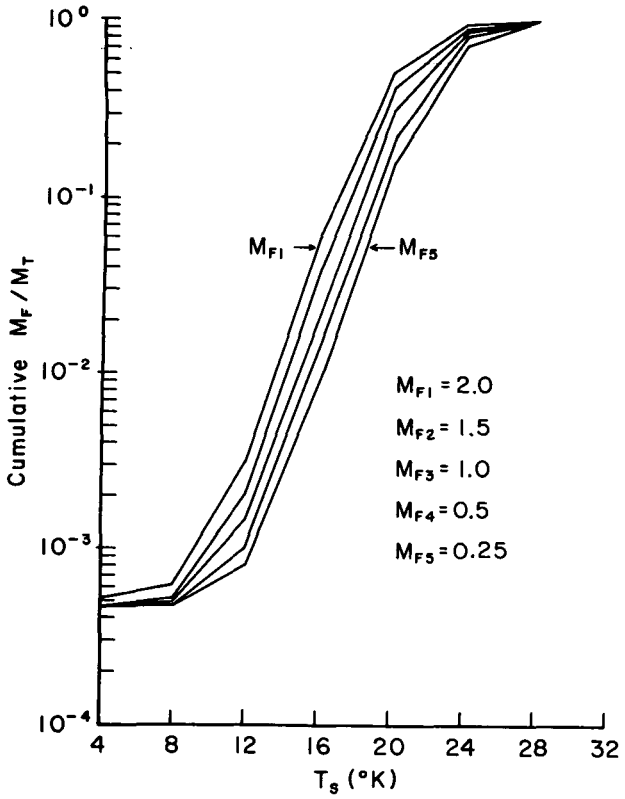

FIGURE 1.—Cumulative fraction of rainwater content, M_F, frozen by heterogeneous nucleation (g·m^{-3}).

prescribed on the basis of the median temperature of the spectral band. In addition to concentration, average mass, a-axis (basal plane axis), and c-axis (prism plane axis) of each spectral band are predicted.

The change in liquid water content $M(D)$ of drops of mass $X(D)$ and diameter $D\pm\delta D/2$ is described by the following equation:

$$\left.\frac{dM(D)}{dt}\right|_{\text{coll}}=X(D)\left.\frac{dN(D)}{dt}\right|_{\text{coll}}. \tag{6}$$

The change in concentration of raindrops of diameter $D\pm\delta D/2$ by collection is described by the so-called kinetic equation of collection. Thus,

$$\left.\frac{dN(D)}{dt}\right|_{\text{coll}}=\frac{-\pi D^2}{4}\sum_{I=1}^{21}(V_D-V_I)E(D|I)n(I)\Delta T(I)N(D) \tag{7}$$

where V_D is the terminal velocity of droplets of diameter D, V_I is the terminal velocity of ice crystals in class I, $E(D|I)$ represents the collision efficiency between drops of diameter D and crystals in class I defined relative to the cross-section, $\pi D^2/4$, and $n(I)\Delta T(I)$ is the concentration of ice crystals in class I.

The change in total rainwater content, M_T, due to collection of ice crystals is, therefore,

$$\frac{dM_T}{dt}=\frac{-\pi^2\rho_l}{24}\int_0^\infty D^5\sum_{I=1}^{21}|V_D-V_I|E(D|I)n(I)\Delta T(I)N(D)dD. \tag{8}$$

If an average collection efficiency, $\overline{E(D|I)}$, is considered and $V_D>V_I$, then eq(8) may be written

$$\frac{dM_T}{dt}=\frac{-\pi^2\rho_l}{24}\left[\left|\sum_I\overline{E(D|I)}n(I)\Delta T(I)\underbrace{\int_0^\infty D^5V(D)N(D)dD}_{\psi_1}-\sum_I V_I\overline{E(D|I)}n(I)\Delta T(I)\underbrace{\int_0^\infty D^5N(D)dD}_{\psi_2}\right|\right]. \tag{9}$$

Replacing $N(D)$ in ψ_1 and ψ_2 by the Marshall-Palmer generating function (Cotton 1971) and $V(D)$ as used by Liu and Orville (1968), we get

$$V(D)=(D_\tau^{a_1/b_1})D^{b_1} \tag{10}$$

where $a_1=2115$ cm/s and $b_1=0.8$. Integrating, we find that

$$\psi_1=(D_\tau^{a_1/b_1})\frac{N_0^{\Gamma(6+b_1)}}{\lambda^{6+b_1}}. \tag{11}$$

Similarly,

$$\psi_2=\frac{N_0^{\Gamma(6)}}{\lambda^6}. \tag{12}$$

In summary, the total change in rainwater content due to collection is

$$\frac{dM_T}{dt}=\frac{-\pi^2\rho_l}{24}\left[\left|\sum_{I=1}^{21}\overline{E(D|I)}n(I)\Delta T(I)\psi_1-\sum_{I=1}^{21}V_I\overline{E(D|I)}n(I)\Delta T(I)\psi_2\right|\right]. \tag{13}$$

The average collection efficiency is calculated with the Langmuir and Blodgett (1945) formula of collision efficiency transformed to include the added geometric cross-section of an ice crystal. Thus, if $\overline{E(D|I)}_L$ represents the efficiency calculated with the Langmuir approximation, then the efficiency including the cross-section of crystal is

$$\overline{E(D|I)}=\overline{E(D|I)}_L\frac{(D+A')^2}{D^2} \tag{14}$$

where $A'=a$ for plates and spherical ice crystals and $A'=(a+c)/2$ for columns and needles. The collection efficiency is computed relative to the droplet corresponding to the average mass of the Marshall-Palmer (1948) distribution.

Change in ice crystal concentration. To maintain water continuity, one must account for the reduction in ice crystal concentration by collection of raindrops. The change in concentration of crystal class I is similar to eq (7); that is,

$$\frac{dn(I)}{dt}=\frac{-\pi\overline{E(D|I)}n(I)}{4}\left[\left|\underbrace{\int_0^\infty D^2V(D)N(D)dD}_{\xi_1}-V_I\underbrace{\int_0^\infty D^2N(D)dD}_{\xi_2}\right|\right]. \tag{15}$$

Defining $N(D)$ and $V(D)$ as was done earlier in this section, we find

$$\xi_1=N_0(D_r^{a_1/b_1})\frac{\Gamma(3+b_1)}{\lambda^{3+b_1}} \tag{16}$$

and

$$\xi_2=\frac{N_0\Gamma(3)}{\lambda^3}. \tag{17}$$

3. DISTRIBUTION OF FROZEN RAINWATER

Once a portion of the rainwater is frozen either by crystal collection or by heterogeneous freezing, the resultant frozen particles can grow predominantly by the accretion of cloud droplets and, in the case of a glaciated cloud, by vapor deposition. To predict the change in frozen water content by either of the above microphysical processes or, in the case of an Eulerian dynamic system, by particle advection, we must describe the distribution of frozen particles. Ideally, one would predict the distribution of frozen particles by solving a system of continuity equations describing the rates of change of the mass or radius spectral density of quasi-spherical, frozen particles. This is, of course, an extremely complex numerical problem.

The approach taken here is to approximate the actual distribution of frozen raindrops by an average, in-cloud size distribution of frozen particles. Unfortunately, the quantity of in-cloud measurements of size distributions of frozen particles is scanty. Actual formulations of the size distribution of such particles are even fewer. The consensus seems to be that frozen particles are distributed approximately according to the inverse exponential form similar to the Marshall-Palmer (1948) distribution.

Jones (1960) analyzed a number of observations taken with aluminum foil samplers. The data included flights by the British Meteorological Research Flight in cumulonimbus clouds in temperate zones and by Britannia aircraft in the Tropics. He found that the concentration of particles per cubic meter of diameter $D\pm\delta D/2$ sampled in the tropical cumuli could be approximated by the formula $N(D)=10^3/D^3$. In the case of the temperate zone samples, he found that $N(D)=10^3/D^{2.3}$ for $D<2$ mm and $N(D)=10^4/D^{5.4}$ for $D>2$ mm. He further demonstrated that the family of curves of size distribution could be approximated by the equation

$$N(D)=N_0e^{-\lambda(D-D_{\min})} \tag{18}$$

where $D_{\min}$ represents the minimum particle diameter considered in the formulation. The above equation essentially represents a truncated Marshall-Palmer (1948) distribution. Jones (1960) chose a minimum particle diameter of 250 μm. Fortunately, this is only 50 μm greater than the minimum diameter of raindrops considered in preceding sections. Because of the change in density during freezing, this gap between the two distributions is further reduced.

4. EVALUATION OF DISTRIBUTION PARAMETERS

Jones (1960) demonstrated that the family of curves of size distribution, stratified according to water content, could be fitted to eq (18) when

$$\lambda=2.67\times10^3M_F^{-1/3} \tag{19}$$

where λ has dimensions of (m^{-1}) and M_F is the water content ($g\cdot m^{-3}$). Equation (19) was found using the assumption that the mean particle density of the distribution is 0.6 $g\cdot cm^{-3}$.

By dimensional analysis, one can argue that, given

$$\lambda=\lambda(\delta_i, N_0, M_F),$$

then

$$\lambda=k\delta_i^{1/3}N_0^{1/4}M_F^{-1/3}. \tag{20}$$

If λ has dimensions of (m^{-1}),

$$N_0=10^{7.1}m^{-4},$$

and

$$\delta_i=0.6\times10^6\ g\cdot m^{-3},$$

then k will have a value of 2.52×10^{-6}.

The total concentration of the distribution of frozen particles can be found by integrating over the entire spectrum. Thus,

$$N_T=\int_0^\infty N_0e^{-\lambda(D-D_{\min})}dD$$

or

$$N_T=N_0/\lambda. \tag{21}$$

Equation (21) is identical to the result obtained by Kessler (1967) for a Marshall-Palmer (1948) distribution.

5. ACCRETION OF CLOUD WATER BY FROZEN RAINDROPS

Once supercooled raindrops have frozen, they grow predominantly by accretion of cloud droplets. Not only does this process increase the size of the precipitation elements, but it also provides a continued source of energy to the cloud through the latent heat of fusion of accreted droplets.

The rate of mass growth of an ice particle of diameter, D, by accretion of cloud droplets having a water content, m, is given by the equation

$$\left.\frac{dX(D)}{dt}\right|_{\text{accr}}=\pi D^2|V_D-V_C|E(D/C)m \tag{22}$$

where $E(D|C)$ is the collision efficiency between the ice particles and cloud droplets, V_D is the terminal velocity of the ice particles, and V_C is that of cloud droplets.

Because accretion of cloud droplets does not change the concentration of frozen precipitation particles, the change in frozen-particle water content caused by accretion is

$$\left.\frac{dM_F}{dt}\right|_{\text{accr}}=\int_0^\infty\pi D^2|V_D-V_C|E(D|C)mN(D)dD. \tag{23}$$

Assuming $V_D\gg V_C$, substituting eq (18) into eq (23), and employing an average collection efficiency $\overline{E(D|C)}$, we have

$$\left.\frac{dM_F}{dt}\right|_{\text{accr}}=\pi mN_0\overline{E(D|C)}\int_0^\infty D^2V(D)e^{-\lambda(D-D_{\min})}dD. \tag{24}$$

Given that frozen particles are spherical and that the drag coefficient is not a function of diameter, the terminal velocity of frozen particles may be expressed as

$$V(D)=C_D^{-1/2}\left(\frac{4\delta_i g}{3\rho_a}\right)^{1/2} D^{1/2} \tag{25}$$

where g represents the acceleration of gravity and ρ_a is the density of air. Macklin and Ludlam (1961) found that the drag coefficient, C_D, for frozen particles varies over the range $0.45 \leq C_D \leq 0.8$. Magono (1954) suggested that C_D for graupel is typically 0.45. The drag coefficient is taken to have the value 0.6 over the distribution.

Substituting eq (25) into (24), we find

$$\left.\frac{dM_F}{dt}\right|_{\text{accr}} = \pi m N_0 \overline{E(D|C)} C_D^{-1/2}\left[\frac{4\bar{\delta}_i g}{3\rho_a}\right]^{1/2}\int_{D_{\min}}^{\infty} D^{2.5} e^{-\lambda(D-D_{\min})} dD. \tag{26}$$

If we let $\phi=(D-D_{\min})$, and

$$\eta=\int_{D_{\min}}^{\infty} D^{2.5} e^{-\lambda(D-D_{\min})} dD, \tag{27}$$

integrating eq (27) by parts gives us

$$\eta=\frac{D_{\min}^{2.5}}{\lambda}+\frac{2.5}{\lambda^2} D_{\min}^{1.5}+\frac{(2.5)(1.5)}{\lambda^3} D_{\min}^{0.5} + \frac{(2.5)(1.5)(0.5)}{\lambda^3}\int_0^{\infty} \frac{e^{-\lambda\phi} d\phi}{(\phi+D_{\min})^{1/2}}. \tag{28}$$

The latter integral was evaluated by Gradshteyn and Ryzhik (1965) as

$$\xi(D_{\min},\lambda)=\int_0^{\infty} \frac{e^{-\lambda\phi} d\phi}{(\phi+D_{\min})^{1/2}}=\sqrt{\frac{\pi}{\lambda}}\, e^{D_{\min}\lambda}[1-\text{erf}(\sqrt{D_{\min}\lambda})]. \tag{29}$$

Thus,

$$\eta=\frac{D_{\min}^{2.5}}{\lambda}+\frac{2.5}{\lambda^2} D_{\min}^{1.5}+\frac{(2.5)(1.5)D_{\min}^{0.5}}{\lambda^3} + \frac{(2.5)(1.5)(0.5)}{\lambda^3}\xi(D_{\min},\lambda). \tag{30}$$

The average collection efficiency is calculated with the Langmuir formula (Langmuir and Blodgett 1945) with respect to the mean mass of the frozen-particle distribution relative to the mean mass of the cloud water distribution.

6. VAPOR DEPOSITION ON FROZEN RAINDROPS

At cloud water contents greater than about 0.5 $g \cdot m^{-3}$, the rate of change of ice-particle water content by accretion of cloud droplets is several orders of magnitude greater than that by vapor deposition. In a glaciated cloud or low liquid water content clouds, however, neglecting the rate of vapor deposition on frozen particles can lead to serious errors, since it can be an important source of energy.

The rate of vapor-deposition growth of an individual frozen particle of mass $X(D)$ and diameter D is, according to eq (39),

$$\frac{dX(D)}{dt}=4\pi C G(T,P) f(\text{Re})(S-1), \tag{31}$$

the terms for which are all discussed in considerable detail in subsection 10a. For spherical particles, $C=D/2$. Thus, eq (31) becomes

$$\frac{dX(D)}{dt}=2\pi D G(T,P) f(\text{Re})(S-1). \tag{32}$$

Because vapor deposition does not change the particle concentration, the change in total ice-particle water content is

$$\left.\frac{dM_F}{dt}\right|_{V_{\text{dep}}} = \int_{D_{\min}}^{\infty} 2\pi D G(T,P) f(\text{Re})(S-1) N(D) dD. \tag{33}$$

Substituting eq (18) into (33) and considering an average ventilation function $\overline{f(\text{Re})}$, we find that the rate of change of water content by vapor deposition is

$$\left.\frac{dM_F}{dt}\right|_{V_{\text{dep}}} = 2\pi G(T,P)\overline{f(\text{Re})}(S-1) N_0 \frac{\Gamma(2)}{\lambda^2}+\frac{D_{\min}}{\lambda}. \tag{34}$$

The ventilation function $\overline{f(\text{Re})}$ is also evaluated relative to the average mass of the distribution.

7. SYSTEM OF PRIMITIVE ICE CRYSTALS

This section concerns itself with a system of ice crystals that are nucleated at the expense of liquid cloud water. Such crystals may originate either by vapor deposition on an active aerosol, which forces evaporation of cloud droplets, or by some mechanism of cloud droplet freezing. The basic development of the ice crystal model was guided by the desire to create a model general enough in scope to be able to simulate the role of the ice phase in supercooled cumuli. Often, such an objective forced many a compromise between the loss of generality and the need to bridge specific gaps in the knowledge of the physical processes considered. Before we discuss the crystal system as a whole, let us first look at the process of growth of individual crystals.

a. Growth of Single Ice Crystals

Based on the laws of Fickian diffusion, the rate of mass growth of an ice crystal is given by the equation

$$\left.\frac{dx_i}{dt}\right|_s = 4\pi C D_v g(\text{Re})[\rho_w - \rho_w(r)] \tag{35}$$

where C represents the capacitance of the crystal corresponding to an electrostatic analog, D_v is the diffusivity of water vapor in air, ρ_w is the vapor density some distance from the crystal, $\rho_w(r)$ is the vapor density at a distance from the surface of the crystal corresponding to the mean free path of a molecule, and $g(\text{Re})$ is the ventilation factor effecting vapor diffusion. The rate of diffusion of heat

away from the crystal is

$$\frac{dQ_D}{dt}=4\pi Cf(\mathrm{Re})K_i(T_r-T) \tag{36}$$

where K_i is the thermal diffusion coefficient, $f(\mathrm{Re})$ is the ventilation factor effecting thermal diffusion, T_r is the temperature at the surface of the crystal, and T is the temperature some distance away.

The crystal is taken to be in thermodynamic equilibrium such that the heat added to the crystal must be liberated to the environment and vice versa. Thus,

$$L_s\frac{dx_i}{dt}\bigg|_s+L_f\frac{dx_i}{dt}\bigg|_R=\frac{dQ_D}{dt} \tag{37}$$

where L_f is the latent heat of fusion, L_s is the latent heat of sublimation, and $dx_i/dt|_R$ is the rate of mass growth of the crystal by riming.

Following a development similar to Byers (1965), we obtain the following equation:

$$\frac{dx_i}{dt}\bigg|_s=\frac{4\pi C(S-1)}{\dfrac{M_wL_s^2}{f(\mathrm{Re})K_iR_aT^2}+\dfrac{R_aT}{g(\mathrm{Re})M_wD_ve_s(T)}}-\frac{\dfrac{M_w}{R_a}L_sL_f\dfrac{dx_i}{dt}\bigg|_R}{f(\mathrm{Re})K_iT^2\left[\dfrac{M_wL_s^2}{f(\mathrm{Re})K_iR_aT^2}+\dfrac{R_aT}{g(\mathrm{Re})M_wD_ve_s(T)}\right]}. \tag{38}$$

Assuming that $g(\mathrm{Re})\approx f(\mathrm{Re})$ and rearranging, we have

$$\frac{dx_i}{dt}\bigg|_s=4\pi C(S-1)f(\mathrm{Re})G(T,P)-F(\dot{x}_R,T,P) \tag{39}$$

where

$$G(T,P)=\frac{1}{\underbrace{\dfrac{M_wL_s^2}{K_iR_aT^2}}_{A_k}+\underbrace{\dfrac{R_aT}{M_wD_ve_s(T)}}_{B_k}}$$

and

$$F(\dot{x}_R\,T,\,P)=\frac{\dfrac{M_w}{R_a}L_sL_f\dfrac{dx_i}{dt}\bigg|_R}{K_iT^2(A_k+B_k)}.$$

Equation (39) is identical to that derived by Byers (1965) with $f(\mathrm{Re})$ approximately unity and with the second term on the right side neglected. The second term, which represents the contribution to the crystal heat balance by the latent heat released during riming, is of little importance in cumulus clouds having liquid water content (LWC) in excess of 1.0 g·m^{-3} because once the term becomes significant the crystal mass growth is dominated by riming. Crystal mass growth rates derived from vapor deposition and riming may be of comparable magnitude, however, in clouds having LWC of a lesser magnitude. The added term can then be important for proper prediction of the onset of graupel formation. After the first 60 s of growth, the ventilation factor is assumed to be nonunity and is formulated similar to Shiskin (1965) as

$$f(\mathrm{Re})=1.0+0.229\sqrt{\mathrm{Re}}. \tag{40}$$

TABLE 2.—*Crystal growth habit as a function of temperature,* T

Temperature range (°C)	Crystal habit
$0 > T > -3.0$	Hexagonal plates
$-3.0 \geq T \geq -5.0$	Needles
$-5.0 > T > -8.0$	Prisms
$-8.0 \geq T > -12.0$	Hexagonal plates
$-12.0 \geq T \geq -16.0$	Hexagonal plates, dendrites
$-16.0 > T \geq -25.0$	Hexagonal plates
$-25.0 > T$	Prisms

b. Crystal Habit

The habit of ice crystal growth by vapor deposition is extremely important in itself and also for crystal riming, collection of rainwater, and crystal aggregation. Unfortunately, there is not complete agreement on the dependence of crystal growth habit on temperature, supersaturation, mode of crystal nucleation, ventilation, and electrical forces. The influence of electrical forces on crystal habit has not been analyzed sufficiently to be considered in this model. There are indications that the mode of crystal nucleation (i.e., sublimation nuclei, freezing, etc.) does influence the habit of young crystals. Schaefer (1968), for example, demonstrated that ice crystals nucleated on silver iodide or lead iodide crystals exhibited habits differing in fine structure from natural ice crystals. Weickmann et al. (1970) have pointed out that crystals that have been nucleated via frozen cloud droplets often exhibit biplanar structures distinct from sublimation-nucleated crystals. However, it appears that the fine structural differences developed during early growth may be lost in the mature stages of crystal growth. In addition, the resolution of the crystal model to be described is not capable of simulating such fine structural distinctions. Of the remaining habit dependences, temperature is by far the dominant parameter. The dependence on supersaturation in our cloud model is restricted to the case of a water-saturated cumulus cloud.

Table 2 summarizes the assumed crystal habit as a function of temperature and is based largely upon the experiments of Hallett and Mason (1958) and Kobayashi (1957, 1960). The most controversial temperature regimes are those warmer than −3°C, where irregular needles have been observed by Nakaya (1954); −15° to −20°C, where spatial dendritic growth is often observed, and −22° to −25°C, where there is a poorly defined transition from hexagonal plate growth to columnar forms.

c. Specific Formulation of the Vapor-Deposition Growth Equations

To integrate eq (39) with time, one must be able to specify the variation in crystal capacitance, Re, and riming rate. Unfortunately, this requires predictive equations for the rates of geometric growth of the crystals. The geometric structure of crystals is described in this model by the length of two linear dimensions and an identification flag to distinguish between dendrites and hexagonal plates.

TABLE 3.—*Formulation of crystal capacitance, geometric growth rates, and vapor-deposited mass density*

Crystal type	Capacitance term	Linear growth rates	Crystal bulk density (g·cm^{-3}) (for vapor deposition only)
Needles	$C=\frac{c}{\ln \frac{4c^2}{a^2}}$	$\frac{da}{dt}=K_N\frac{dc}{dt}$ $K_N=0.08$	$\delta_i=0.2$
Prisms	$C=\frac{ce}{\ln\left(\frac{1+e}{1-e}\right)}$ $e=\sqrt{1-\frac{a^2}{c^2}}$	$\frac{da}{dt}=K_P\frac{dc}{dt}$ $K_P=0.33$	$\delta_i=0.35$
Hexagonal plates	$C=\frac{ae}{2\sin^{-1}e}$ $c<30\ \mu m$ and $C=\frac{a}{\pi}$ $c\geq 30\ \mu m$ $e=\sqrt{1-\frac{c^2}{a^2}}$	$\frac{dc}{dt}=K_{HP}\frac{da}{dt}$ $K_{HP}=0.12$ $\frac{dc}{dt}=0$	$\delta_i=0.9$
Dendrites	$C=\frac{a}{\pi}$ $c\geq 30\ \mu m$	$\frac{da}{dt}=\frac{dx_i}{dt}\Big/2ka$ $k=38\times10^{-5}g^{-2}$	$0.162\leq\delta_i\leq0.9$
Graupel ($a=c$)	$C=\frac{a}{2}$	$\frac{dc}{dt}=\frac{da}{dt}$	$\delta_i=0.9$
Columnar crystals advected into planar regimes	$C=\frac{ce}{\ln\left(\frac{1+e}{1-e}\right)}$ $e=\sqrt{1-\frac{a^2}{c^2}}$	$\frac{dc}{dt}=0$	$\delta_i=0.9$
Planar crystals advected into columnar regimes	$C=\frac{a}{\pi}$	$\frac{da}{dt}=\frac{dc}{dt}$	$\delta_i=0.9$

The rates of growth of the prism axis of length c, the basal plane axis of length a, and the bulk crystal density are specified on the basis of the data of Magono (1954), Nakaya (1954), Bashkirrova et al. (1964), Todd (1964), Magono and Lee (1966), and Ono (1969).

Table 3 summarizes the assumed crystal capacitance, linear growth rates, and bulk density of vapor-deposited ice. The author intends to update the assumptions regarding the crystal geometric structure with some of the recent data discussed by Ono (1970). We assumed here that the early stages of dendritic growth are identical to that of hexagonal plates. After a hexagonal plate grows to a thickness of 30μm and is in the temperature range $-12\geq T\geq-16$°C, the crystal is allowed to grow two-dimensionally in the dendritic configuration.

d. Crystal Growth by Riming

To simulate the growth of primitive ice crystals by riming, we adopted a simple accretion model. The mass growth of a crystal by riming is then

$$\left.\frac{dx_i}{dt}\right|_R=A_i'(V_i-V_c)Em \tag{41}$$

where A_i' represents the geometric capture cross-section, V_i is the terminal velocity of the crystal, V_c is the terminal velocity of the cloud droplet contributing the most to the LWC, E is the collection efficiency, and m is the LWC of the cloud. Given that a crystal always falls in a direction normal to the plane of its major dimension, $A_i'=ac$ for needles and columns, and $A_i'=\pi a^2/4$ for plates, dendrites, and spherical ice particles.

Geometric growth by riming is assumed to be in the direction of the a-axis for needles and columns and in the direction of the c-axis for plates and dendrites. Once a crystal has rimed to the extent that the a- and c-axes are of comparable size, the crystal is then considered to be a spherical graupel with corresponding geometric cross-section, fall velocity, and collection efficiency. The density

of growth by riming, δ_R, is estimated from the data of Nakaya (1954) to be 0.12 g·cm^{-3}. The work of Macklin (1962) suggests that the density of rimed substance is a function of the accreted cloud droplet radius and the impact velocity and surface temperature of the crystal. However, the empirical formula he developed from his experiments is both cumbersome and out of the range of conditions for small ice crystal riming.

The coalescence efficiency is defined to be unity throughout this study. Hydrodynamic collision efficiencies are estimated from the meager theory and data available for simple cylinders, disks, and spheres. The collision efficiencies are calculated relative to the cloud droplet having the mean mass of the distribution. Cylinder efficiencies are estimated from the computations of Davies and Peetz (1956) for viscous and transition flow. The hydrodynamic efficiencies for simple hexagonal plates are calculated by using the simplified theory of Ranz and Wong (1952) for inertial impaction on disks. Dendrite efficiencies are modified somewhat to account for the effect of branching in reducing the geometric cross-section to less than that for a solid disk. Thus, for dendrites having an a-axis greater than 250 μm, the collection efficiency is calculated using the equation

$$E_a=\frac{a_{HP}^2E_{HP}+K_D(a^2-a_{HP}^2)}{a^2} \tag{42}$$

where a_{HP}^2 E_{HP} represents the effective geometric cross-section of a 250-μm diameter hexagonal plate kernel, and K_D is the fraction of the remaining cross-section filled with crystal substance. The coefficient K_D is taken to be 0.5. Collision efficiencies of spherical collectors are computed with the approximate formula developed by Langmuir and Blodgett (1945) for potential flow about a sphere.

e. Crystal Terminal Velocity

The fall velocity of needle crystals is based on the data of Nakaya (1954). However, to take into account the variation in terminal velocity with height and the effects of riming, we determined the behavior of the drag coefficient (C_D) as a function of Reynolds number (Re) from the Nakaya (1954) data and the modeled crystal mass and geometry. Under these conditions, the relationship was found to be of the form

$$C_D=\frac{\mathrm{Re}}{A+B(\mathrm{Re})};\qquad 0.5\leq\mathrm{Re}\leq3.0 \tag{43}$$

where $A=-0.49$, and $B=1.65$. By equating the aerodynamic drag force to the force of gravity and rearranging terms, the terminal velocity of a needle may then be found by solving the cubic equation

$$V_T^3=\left(\frac{\pi\delta_i gBa}{2\rho_a}\right)V_T-\left(\frac{\mu a\pi\delta_i gA}{2\rho_a}\right)=0 \tag{44}$$

where δ_i is the total crystal density, g is the acceleration of gravity, ρ_a is the density of air, and a is the length of the crystal basal plane axis. The terminal velocity of columnar crystals was derived from the C_D versus Re relationships determined by Podzimek (1968) for laboratory-modeled columns; the terminal velocity of hexagonal plates was derived from the C_D versus Re relationships for a cylindrical disk similar to Shiskin (1965).

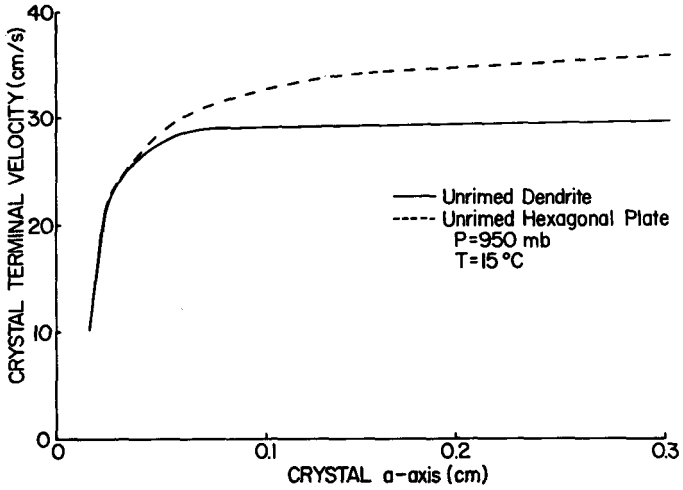

FIGURE 2.—Predicted terminal velocity versus major dimension of an unrimed hexagonal plate and a modeled dendrite.

The problem of determining the fall velocity of dendritic crystals is much more difficult than would first appear. Nakaya (1954) reported that the terminal velocity of unrimed dendrites is nearly constant at 30 cm/s. However, the growth model described above adds two complications to this simple observation. First, the model predicts that dendrites develop from a hexagonal plate kernel. It is necessary, therefore, to estimate the transition in terminal velocity from that of a hexagonal plate to that of an unrimed dendrite. Second, it is desirable to estimate the variation in terminal velocity of a dendrite resulting from riming.

The first problem was solved by linear interpolation between the computed terminal velocity of the modeled hexagonal plate kernel and the constant terminal velocity of a pure unrimed dendrite. This curve is shown in figure 2. Based on the modeled crystal mass, geometry, and the assumed transitional terminal velocity, the corresponding C_D versus Re relationship was computed as shown in figure 3. The best fit to this curve is of the form

$$C_D=\alpha_1+\frac{\beta_1}{\mathrm{Re}}+\frac{\nu_1}{(\mathrm{Re})^2} \tag{45}$$

where $\alpha_1=0.86$, $\beta_1=1.48$, and $\nu_1=111.97$.

Solving for the terminal velocity of a dendrite, we find that

$$V_T=\frac{-\beta_1\mu a+\sqrt{\beta_1^2\mu a^2-4\alpha_1\nu_1\mu_a^2+8\rho_a\alpha_1a^2c\delta_i g}}{2\rho_a\alpha_1 a},\qquad c>30\mu m. \tag{46}$$

Furthermore, if it is assumed that riming does not alter the above C_D versus Re curve, eq (46) can be applied to rimed crystals. The latter assumption is justified for light riming because riming growth of dendrites is largely in

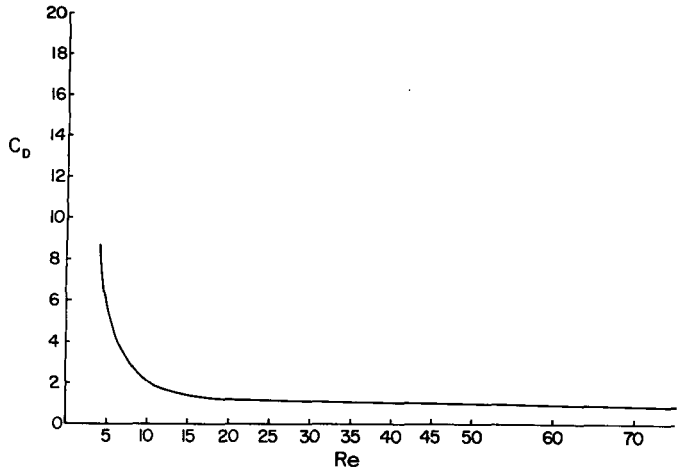

FIGURE 3.—Estimated variation of the drag coefficient as a function Reynolds number for modeled dendrites.

the direction of the c-axis (which is taken to be parallel to the flow axis) rather than in the direction of the a-axis (which would fill in the branched structure and alter C_D of the crystal).

The terminal velocity of crystals or ice particles having a ratio of large to small axes of less than 1.1 and having an Re <20.0 is computed using a technique discussed by Fuchs (1964). Fall velocities of similar crystals having a larger Re are computed under the assumption that they are spherical.

f. Integration of the Crystal Growth Equations

All growth equations are initialized by a 60-s, analytic integration of the sublimation equations. The analytic integration is performed with the additional restriction that the ratio a/c is a constant. Further integrations are accomplished numerically by centered differences. Both growth by riming and vapor-deposition growth of all crystal forms are computed following the 60-s initialization. A variable integration time step of roughly 5 s was found to keep truncation errors at a minimum.

g. Spectrum of Ice Crystals

To predict the distribution of water substance on a system of growing ice crystals, one must identify the concentration of ice crystals of a given mass and geometric structure. In the case of liquid cloud or raindrops, one can employ a spectral density function of an internal particle parameter such as droplet mass or diameter. In this case, since they are nearly spherical, there is a one-to-one correspondence between the mass of the droplet and its dimension. However, an ice particle of mass x may have an a-axis of length a_1 and a c-axis of length c_1 or nearly an infinite number of combinations of axis lengths and still have mass x. The obvious solution is to employ a spectral density function of x, a, and c. Storing, manipulating, and solving continuity equations of a three-dimensional spectral function is rather difficult. It was therefore decided

TABLE 4.—*Classification of the spectrum of ice crystals as a function of nucleation temperature*

Crystal class index (I)	Median temperature $T_*(I)$	Spectral width (ΔT)
	(°K)	(°K)
1	272.4	1.5
2	270.9	1.5
3	269.15	2.0
4	267.40	1.5
5	265.90	1.5
6	264.15	2.0
7	262.15	2.0
8	260.15	2.0
9	258.15	2.0
10	256.4	1.5
11	254.9	1.5
12	253.4	1.5
13	251.9	1.5
14	250.4	1.5
15	248.9	1.5
16	247.9	2.0
17	245.9	2.0
18	243.9	2.0
19	241.9	2.0
20	239.9	2.0
21	237.9	2.0

to use a nice crystal spectral function of an external parameter. Because the crystal habit and the concentration of crystals are largely functions of temperature, the obvious external parameter should be nucleation temperature.

One of the primary conditions that must be met when employing an ice crystal spectral density function of nucleation temperature is that the spectral bands be defined such that only a single habit of growth is nucleated within the band. To satisfy this condition, each range of temperature having a common crystal habit as shown in table 2 is subdivided into temperature bands having a width of 1.5°–2.0°C. The spectral density of crystals nucleated in each band is predicted on the basis of the median temperature of the interval. Strictly speaking, the term "spectral density" must be used quite loosely with regard to the concentration of crystals in each band. In essence, we are describing the concentration, mass, and geometry of several independent monodisperse distributions of ice crystals for which the major distinguishing feature is the point of origin both in time and in geometric space. This point of origin is referenced to a given range of nucleation temperature. Table 4 summarizes the resulting 21-element, discrete spectral distribution of ice crystals.

8. CLOUD MODEL

The cloud dynamic framework treated in this and succeeding sections can be considered to be two different physical models in one. The first model is the steady-state jet model that can be traced to the work of Weinstein and Davis (1968), Squires and Turner (1962), and originating with the work of Stommel (1947). The second dynamic model is essentially a simulation of the Experimental Meteorology Laboratory (EML) spherical vortex model described by Simpson and Wiggert (1969). Conceptually,

it is considered that one is tracing the life history of a rising parcel of air or the center of mass of a spherical vortex that is interacting with its environment by "entraining" unperturbed environmental air. The physical process of entrainment changes the total water continuity, affects the thermodynamic structure, and alters the momentum of the rising convective element. In the case of the steady-state model, the Lagrangian predictions are interpreted to represent a steady-state vertical cloud profile of water mass, temperature, and momentum that has formed during the growth stage of cumulus convection. The EML spherical vortex calculations, on the other hand, are interpreted to represent the internal cloud properties located at the center of mass of a spherical vortex cloud.

a. Moisture Continuity

The total moisture mixing ratio, Q_T, of the modeled cloud is assumed to be the sum of five phase components. Thus,

$$Q_T=q_v+Q_c+Q_H+Q_F+Q_I \tag{47}$$

where q_v is the cloud vapor mixing ratio, Q_c is the cloud water mixing ratio, Q_H is the mixing ratio of rainwater, Q_F is the mixing ratio of frozen hydrometeor water, and Q_I is the mixing ratio of the class of ice particles that have nucleated at the expense of Q_c.

In the rising cloud parcel, the only sources or sinks of Q_T are the result of its mixing with the environment and the net fallout of precipitation from the parcel. Hence,

$$\frac{dQ_T}{dz}=\frac{dq_v}{dz}+\frac{dQ_c}{dz}+\frac{dQ_H}{dz}+\frac{dQ_F}{dz}+\frac{dQ_I}{dz} -\mu(q_v-q_e+Q_c+Q_H+Q_F+Q_I)-\text{fallout} \tag{48}$$

where q_e is the environmental vapor mixing ratio, μ is the entrainment parameter, and the last term represents the rate of fallout of precipitation as described in subsection 8f.

The entrainment parameter represents the fractional change in cloud mass, M, with height; that is,

$$\mu=\frac{1}{M}\frac{dM}{dz}. \tag{49}$$

It is assumed that the cloud does not become supersaturated with respect to water. Thus, the continuity equation for q_v is

$$\frac{dq_v}{dz}=\frac{dq_s}{dz}-\mu(q_v-q_e) \tag{50}$$

where q_s is the saturation mixing ratio with respect to water. Applying the Clausius-Clapeyron equation to a parcel cooling moist adiabatically with sensible heat mixing, we find that

$$\frac{dq_s}{dz}=\frac{\epsilon L_c q_s}{R_a T^2}\left(\frac{dT}{dz}\right)+\frac{g}{R_a T_0}q_s \tag{51}$$

where dT/dz is calculated with eq (64) discussed in subsection 8c. When Q_c is less than an arbitrary threshold [Q_c (min) in a supercooled cloud], the cloud is assumed to be glaciated and is not allowed to become supersaturated with respect to ice. Thus, the continuity equation of q_v for a glaciated cloud is

$$\frac{dq_v}{dz}=\frac{dq_{si}}{dz}-\mu(q_v-q_e) \tag{52}$$

where q_{si} is the saturation mixing ratio with respect to ice. The vertical change in q_{si} is calculated with eq (51), the latent heat of condensation, L_c, being replaced by the latent heat of sublimation, L_s; q_s is replaced by q_{si}; and dT/dz is evaluated with eq (70).

The threshold Q_c(min) is presently taken to be 0.01 g/kg. The continuity equation for Q_c is

$$\frac{dQ_c}{dz}=-\frac{dq_s}{dz}-\mu Q_c-\text{conv}-\text{accr}\,(Q_H) -\text{accr}\,(Q_F)-\text{riming}-\text{subl.} \tag{53}$$

The first term on the right side of eq (53) represents the production of Q_c by condensation. The second term represents the dilution of Q_c by entrainment of clear air. The third term represents the conversion of cloud droplets to liquid hydrometeors,

$$\text{conv}=\frac{\left.\frac{dM}{dt}\right|_{\text{auto}}}{w},$$

and is described by eq (18) in Cotton (1972) with the liquid water content transformed into mixing ratio; w is the cloud updraft velocity. The fourth term on the right side of eq (53) represents the accretion of Q_c by Q_H,

$$\text{accr}\,(Q_H)=\frac{\left.\frac{dM}{dt}\right|_{\text{accr}}}{w},$$

described by eq (3) in Cotton (1972), with the water contents again transformed into mixing ratios. Similarly, the fifth term on the right side of eq (52) represents the accretion of Q_c by Q_F described by eq (41) also transformed to mixing ratios.

The last two terms in eq (53) represent the growth of Q_I by ice crystal riming and vapor deposition at the expense of Q_c. If the ice crystal spectral density is in dimensions of $\text{cm}^{-3}\cdot(^\circ\text{K})^{-1}$,

$$\left.\frac{dQ_c}{dt}\right|_{\text{riming+subl}}=-\frac{1}{\rho_a}\frac{d}{dt}\left[\sum_{J=1}^{21}\Delta T(J)n(J)\overline{X(J)}\right]. \tag{54}$$

Since crystal growth by riming and vapor deposition does not change the spectral density of crystals, then

$$\left.\frac{dQ_c}{dz}\right|_{\text{riming+subl}}=-\frac{1}{\rho_a w}\left[\sum_{J=1}^{21}\Delta T(J)n(J)\dot{\overline{X(J)}}\right] \tag{55}$$

where $\dot{\overline{X(J)}}$ is calculated with the use of the ice crystal model described in section 7 and w is the updraft velocity.

Similarly, the continuity equation of Q_H is

$$\frac{dQ_H}{dz}=-\mu Q_H+\text{conv}+\text{accr}\ (Q_H)-\text{freezing}-\text{fallout}\ (Q_H) \tag{56}$$

where the fourth term represents the freezing of Q_H by heterogeneous nucleation and crystal collection as expressed by eq (5) and (13), which have been transformed to water mixing ratios and spatial derivatives.

The continuity equation of Q_F is

$$\frac{dQ_F}{dz}=-\mu Q_F+\text{freezing}+\text{accr}\ (Q_F)+\text{subl}\ (Q_F)+\text{coll}\ (Q_I)-\text{fallout}\ (Q_F) \tag{57}$$

where the fourth term represents the vapor-deposition growth on the frozen particles predicted by eq (34), which has been transformed to mixing ratio. The fifth term represents the mass added to those raindrops that have collected ice crystals. Since raindrop collection of ice crystals changes only the concentration of the latter,

$$\frac{dQ_F}{dz_{\text{coll}}}=\frac{1}{\rho_a w}\sum_{J=1}^{21}\overline{X(J)}n(\dot{J})\Delta T(J) \tag{58}$$

where $n(\dot{J})$ is calculated with eq (15). Finally, the continuity equation of Q_I is

$$\frac{dQ_I}{dz}=\text{riming}+\text{subl}+\text{coll}(Q_I)-\mu Q_I-\text{fallout}\ (Q_I). \tag{59}$$

A major change in the model since previous reportings (Cotton 1970) is that the ice crystal model is disconnected from the thermodynamic system once the cloud becomes glaciated. The change in ice mixing ratio by vapor deposition in a glaciated cloud is then

$$\text{Subl}=-\frac{dq_{si}}{dz}. \tag{60}$$

The change was necessary because we found in subsequent calculations that truncation errors in the microphysical model linked to the thermodynamic-vapor continuity equations forced the thermodynamic system away from an ice adiabat. Calculations with the ice crystal model can be continued, however, by solving for the cloud supersaturation in the equation,

$$\frac{N_T\dot{\bar{x}}}{\delta_a w}=-\frac{dq_{si}}{dz}, \tag{61}$$

where

$$\dot{\bar{x}}=4\pi\bar{C}G(T,P)(S-1),$$

N_T is the total crystal concentration, and $\bar{C}$ is the average capacitance of the distribution of crystals.

b. Continuity of Ice Nuclei

If artificial ice nuclei are introduced at cloud base or if the spectral distribution of natural ice nuclei is considerably different from that of the cloud environment aloft, continuity equations predicting the variation in the spectral density of ice nuclei, $n(J)$, must be solved. The equation of continuity of the spectral density of ice nuclei rising in an entraining steady-state cloud updraft of radius R is

$$\frac{d}{dz}[n(J)]=-\mu[n(J)-n_e(J)]. \tag{62}$$

Integrating eq (62) through a layer of finite thickness Δz, expanding the exponent, and dropping higher ordered terms, we find

$$n_2(J)=n_1(J)-[n_1(J)-n_e(J)]\mu\Delta z. \tag{63}$$

In the case of natural clouds, $n_e(J)\approx n(J)$ (unless an intense vertical gradient of nuclei concentration exists in the free atmosphere); thus, mixing will have little effect on the concentration of nuclei. In a seeded cloud, however, $n(J)>>n_e(J)$. Hence, entrainment may lead to significant reductions in the concentration of ice nuclei.

c. Cloud Thermodynamics

The equation for the vertical lapse in temperature of a water-saturated cloud is similar to that employed by Weinstein and Davis (1968). Thus,

$$\frac{dT}{dz}=\frac{-\frac{g}{c_p}\left(\frac{L_c q_s}{R_a T}+1\right)-\mu(T-T_e)+\frac{L_f}{c_p}\frac{dQ_f}{dz}+\frac{L_f}{c_p}\frac{dQ_I}{dz}}{1+\frac{\epsilon L_c^2 q_s}{c_p R_a T^2}}. \tag{64}$$

Equation (64) differs from that used by Weinstein and Davis (1968) in that the term $-\mu(L_c/c_p)(q_{s2}-q_e)$ is not explicitly treated. Weinstein and Davis (1968) assumed that the cloud was exactly saturated following integration of eq (64) with the above term included. In addition, the loss of q_v due to mixing was exactly compensated by the evaporation of Q_c in the amount $\Delta Q_c=-\mu(q_{s2}-q_e)\Delta z$, where q_{s2} is the saturation mixing ratio of the cloud following integration of eq (64) with the term in question included. Because q_{s2} is a function of temperature, the amount of cloud evaporation is, in fact, an overcompensation. Thus, their technique of cloud saturation adjustment following vapor mixing results in a cloud that is cooler and drier than it should be. To correct this error, we employed a technique of adjusting the cloud isobarically to saturation similar to that developed by Murray (1970). Suppose that T_2, q_{v2}, Q_{c2}, and $q_{s2}=q_{s2}(T_2)$ represent the predicted cloud properties found by integrating eq (63), (50), and (53) over a depth, Δz, and using the Clausius-Clapeyron equation, respectively.

The adjustment to water saturation will be made isobarically; thus,

$$\delta q_s=\frac{\epsilon L_s q_s}{R_a T^2}\delta T. \tag{65}$$

The heat required to adjust the cloud to water saturation is

$$\delta h=L_c\delta q_v=(c_p+q_v c_{pv}+Q_c c_w)\delta T \tag{66}$$

where c_{pv} is the specific heat of moist air at constant pressure and c_w is the heat capacity of water. Therefore, the change in cloud temperature due to saturation adjustment is

$$\delta T=-\frac{L_c\delta q_v}{c_p+q_vc_{pv}+Q_cc_w}. \tag{67}$$

We wish to adjust the vapor mixing ratio such that the final vapor mixing ratio is equivalent to the final saturation mixing ratio. Thus,

$$q_{v2}+\delta q_v=q_{s2}+\delta q_s. \tag{68}$$

Substituting eq (65) and (67) into eq (68) and rearranging, we find that

$$\delta q_v=-\frac{(q_{v2}-q_{s2})}{1+\left[\frac{\epsilon L_c^2q_{s2}}{R_aT^2(c_p+q_vc_{pv}+Q_cc_w)}\right]}. \tag{69}$$

To accomplish this adjustment, the amount of Q_c that must be evaporated is $\delta Q_c=-\delta q_v$. Upon the completion of this procedure, the cloud should be exactly saturated.

The vertical lapse in temperature in a glaciated cloud is

$$\frac{dT}{dz}=\frac{-\frac{g}{c_p}\left(\frac{L_sq_{si}}{R_aT}+1\right)-\mu(T-T_e)+\frac{L_f}{c_p}\frac{dQ_F}{dz}}{1+\frac{\epsilon L_i^2q_{si}}{c_pR_aT^2}}. \tag{70}$$

The glaciated cloud is adjusted to ice saturation using a procedure identical to that described for a water-saturated cloud except that the appropriate latent heats and saturation mixing ratios are determined with respect to ice.

d. Dynamics

The development of the vertical equation of motion used in the model is based on the derivation by Squires and Turner (1962). The vertical change in momentum flux due to buoyancy forces is

$$\frac{d}{dz}(\pi R^2w^2\rho_a)=\pi R^2g\rho_a\left(\frac{\rho_e-\rho_a}{\rho_a}-Q_s\right) \tag{71}$$

where ρ_a represents the density of the parcel, ρ_e represents the density of the air, and Q_s is the total mixing ratio of condensed water substance.

If we make use of the definition of virtual temperature and the equation of state of moist air and rearrange terms, eq (71) becomes

$$w\frac{dw}{dz}=g\left(\frac{T_{vc}-T_{ve}}{T_{vc}}-Q_s\right)-\mu w^2. \tag{72}$$

If we let

$$F_\alpha=\left(\frac{T_{vc}-T_{ve}}{T_{ve}}-Q_s\right)g$$

and

$$K_\alpha=2\mu,$$

eq (72) may be integrated analytically from z_1 to z_2, assuming F_α and K_α are constant in the layer. Hence,

$$w_2=\left[\frac{2F_\alpha}{K_\alpha}+\left(w_1^2-\frac{2F_\alpha}{K_\alpha}\right)\exp(-K_\alpha\Delta z)\right]^{1/2}. \tag{73}$$

To simulate the EML spherical vortex model, we modified the forcing term, F_α, by the addition of the virtual mass coefficient, γ. Thus,

$$F_\alpha=\frac{\left(\frac{T_{vc}-T_{ve}}{T_{ve}}-Q_s\right)g}{1+\gamma}$$

where γ is taken to be 0.5, similar to Simpson and Wiggert (1969).

e. Variation in Updraft Radius

The updraft radius of the EML simulated model is simply maintained constant. In the case of the steady-state model, however, the updraft radius is varied to maintain continuity of updraft mass flux. Writing the continuity equation of updraft mass flux in logarithmic form, we find

$$\frac{d}{dz}(\ln R)=\frac{\mu}{2}-\frac{1}{2}\frac{d}{dz}\ln(\rho_aw). \tag{74}$$

If we integrate eq (74) from z_1 to z_2, the cloud updraft radius at z_2 becomes

$$R_2=R_1\left(\frac{\rho_1w_1}{\rho_2w_2}\right)^{1/2}\exp(0.5\mu\Delta z). \tag{75}$$

One must be cautious in interpreting the predicted updraft radius in terms of the physical appearance of a cloud. The active portion of the cloud, which the predicted radius is interpreted to represent, is often only a small fraction of the apparent cloud radius. Davis et al. (1967) suggest that the updraft radius is roughly one-half of the cloud radius.

f. Precipitation Fallout

Clearly, one of the most difficult problems that arises when one wishes to compare modified Lagrangian parcel calculations with actual cloud observations is how to predict that portion of hydrometeor water that is transported to a given level in a cloud.

Simpson and Wiggert (1969) have proposed a simple scheme of precipitation fallout from a spherical cloud bubble of radius R. That is, the fractional fallout of precipitation in each vertical integration is the ratio of the time for the tower to rise through a vertical depth, Δz, to the time for the median-volume diameter drop to fall through one radius. This scheme is employed in the simulated EML spherical vortex model calculations.

Applying the Simpson and Wiggert (1969) fallout scheme to a steady-state cloud, however, is conceptually inconsistent with the steady-state jet interpretation of the Lagrangian profile. The characteristic vertical depth, R, has no meaning in the case of the jet interpretation. Weinstein and Davis (1968) proposed that all precipitation should be released from a steady-state jet when the terminal velocity of the median-volume diameter exceeded the updraft velocity. The median-volume diameter fall velocity rarely exceeds 4 to 5 m/s. Thus, precipitation is carried along until the updraft is nearly destroyed.

Howell and Lopez (1968) suggested a unique approach that is quite applicable to the steady-state interpretation. Their scheme, which they call the "waterwheel," is to simply drop out that portion of water [distributed in a Marshall-Palmer (1948) distribution] that has a terminal velocity in excess of the updraft velocity, w. If D_w represents the raindrop diameter falling at a terminal velocity equivalent to the updraft velocity, then the water content that the cloud parcel leaves behind is

$$M_H(>D_w)=\int_{D_w}^{\infty}\frac{\pi\rho_l D^3}{6}N_0e^{-\lambda D}dD \tag{76}$$

or

$$M_H(>D_w)=M_T\left(\frac{D_w^3\lambda^3}{6}+\frac{D_w^2\lambda^2}{2}+D_w\lambda+1\right)e^{-\lambda D}w. \tag{77}$$

The critical or cutoff diameter is calculated with the help of the fall velocity equation discussed by Cotton (1972):

$$D_w=\left(\frac{w}{a_1}\right)^{1/b_1}. \tag{78}$$

Equation (77) may be transformed into rainwater mixing ratios and cgs dimensions by replacing $M_H(>D_w)$ and M_T by Q_H $(>D_w)$ and Q_{HT} and defining D_w in (cm) and λ in (cm^{-1}).

One can apply a similar philosophy to the case of the water density of frozen particles, M_F, exceeding the equilibrium diameter, D_w:

$$M_F(>D_w)=\int_{D_w}^{\infty}\frac{\pi D^3}{6}\rho_i N_0e^{-\lambda(D-D_{\min})}dD. \tag{79}$$

Integrating eq (79) by parts, we find

$$M_F(>D_w)=\frac{\pi\rho_i N_0e^{-\chi}}{6}\left[\frac{1}{\lambda^4}(\chi^3+3\chi^2+6\chi+6)+\frac{3D_{\min}}{\lambda^3}(\chi^2+2\chi+1)+\frac{3D_{\min}^2}{\lambda^2}(\chi+1)+\frac{D_{\min}^3}{\lambda}\right] \tag{80}$$

where $\chi=\lambda(D_w-D_{\min})$. The equilibrium diameter is calculated with eq (27) in the form

$$D_w=\left[\frac{3\rho_a C_D}{4\rho_i}\right]w^2. \tag{81}$$

The same approach is extended to the ice crystal spectra by scanning and dropping out those members having a terminal velocity in excess of the updraft velocity.

9. NUMERICAL PROCEDURE

Before model calculations are begun, a raw data upper air sounding is read into a computer and interpolated onto a log pressure scale (Weinstein and Davis 1968) from cloudbase to the top of the sounding in uniform vertical increments of length Δz. The vertical increment Δz is taken to be 100 m in the numerical experiments described here.

Following interpolation, a set of boundary conditions is prescribed that includes the entrainment constant, k^1 (where $\mu=k^1/R$), the initial updraft radius, R_0, the initial temperature perturbation, ΔT, and the initial updraft velocity, w_1. Unless otherwise specified, k^1 is taken to be 0.2, $\Delta T=0.0$°C, and $w_1=200$ cm/s. for temperate-zone continental clouds. To simulate maritime tropical cumulus, we chose the initial updraft velocity to be in the range $50< w_1 < 125$ cm/s.

Next, a set of cloud microphysical parameters is defined. The initial cloud droplet concentration is prescribed to predict the average droplet mass. Because the conversion parameterization described by Cotton (1972) requires a different set of equations for the coefficients, depending on the colloidal stability, these are defined internally.

The cumulative concentration $N(I)$ of ice crystal nuclei is then specified with

$$N(I)=\int_{T_s=0}^{T_s(I)}f(T)dT \tag{82}$$

where $f(T)$ represents the concentration of ice crystals nucleated over the temperature range T to $T\pm dT/2$, and $T_s(I)$ is specified in table 4.

The cumulative concentration is predicted on the basis of efficiency curves for artificial nuclei generators or seeding material (sec. 10) or, unless otherwise stated, with the exponential nuclei equation discussed by Fletcher (1962),

$$N(T_s)=N_se^{\beta_s T_s}, \tag{83}$$

where β_s and N_s are assumed to be 0.6 and 10^{-5} l^{-1} (i.e., 10^{-5} liter $^{-1}$). The spectral density of crystals nucleated in each spectral band is predicted with the equation

$$n(I)=\frac{[N(I)-N(I-1)]}{\Delta T(I)}. \tag{84}$$

Strictly speaking, eq (84) is an approximation to the exact spectral density,

$$n(I)\Delta T(I)=\int_{T_s(I)-\Delta T(I)/2}^{T_s(I)+\Delta T(I)/2}f(T)dT, \tag{85}$$

but because of the difficulty of specifying $n(I)$ to better than an order of magnitude accuracy, the approximate form is justified. Except for the multiplication experiments described in section 10, the spectral density of ice crystal nuclei characteristic of the natural cloud environment is described by eq (83) as well.

Finally, the cumulative concentration of rainwater freezing nuclei, $K(T_s)$, is prescribed. Unless either an actual data sample or a climatologically averaged spectrum is available, the spectrum is computed with eq (1) and the background coefficients described in subsection 2a.

Following the specification of all boundary conditions and cloud microphysical parameters, the cloud parcel is integrated vertically in height steps, Δz. All integrations of moisture continuity equations and vertical lapses in cloud temperature are performed numerically with a simple first-order integration. Thus, if ξ_i represents a moisture continuity variable (e.g., mixing ratio Q_c) or

temperature at level i, then the predicted variable at level $i + 1$ is

$$\xi_{i+1}=\xi_1+\frac{d\xi}{dz}\Delta z. \qquad (86)$$

Upon completion of this integration, the cloud is then adjusted to water saturation. The cloud vertical velocity is predicted by analytic integration in the layer with eq (73). Similarly, in the case of the steady-state model calculation, the updraft radius is predicted by analytic integration with eq (75). The vertical integration is repeated until the cloud becomes supercooled or the updraft velocity vanishes.

Once the cloud becomes supercooled, the modules predicting the changes in Q_F and Q_I are activated. Because the change in Q_I is predicted by numerical time integration of the ice-crystal growth model described in section 2b, the sum of the microphysical time steps of approximately 5 s is exactly meshed with the time it takes a parcel to rise through the depth Δz. If the vertical change in Q_F and Q_I does not reduce the available Q_c below the glaciation threshold, Q_c(min), the procedure followed is to estimate the water condensed by eq (52) and the vertical lapse in cloud temperature with eq (63).

Once the available Q_c is reduced below the glaciation threshold, the cloud is defined to be glaciated and the ice crystal model is disconnected from the thermodynamic system. The cloud is then assumed to follow an ice adiabat between integration levels and the calculation is analogous to the mixed moist-adiabatic calculation employed for warm clouds. This procedure is continued until the updraft or cloud vertical rise rate vanishes.

10. RESULTS AND DISCUSSION

One of the principal objectives of this study is to determine if the cloud-microphysical model described in preceding sections, with a proper specification of the spectrum of ice crystals, is able to simulate both the colloidal effects of seeding during the growth stage of cumulus convection and the thermodynamic response as well. To meet this objective, we have chosen two observational case studies during which clouds were seeded to enhance their dynamic growth.

The first case study occurred on May 19, 1965, in central Pennsylvania and is discussed by Davis et al. (1967). Cloud bases in the area were observed at 1.8 km above mean sea level (MSL) and tops extended from 4.75 to 5.5 km. Three pyrotechnic flares were released through the center of a 1.75-km-radius cloud. Following seeding, the cloud was observed to grow to an altitude of about 9.15 km and was observed to have grown laterally to a diameter of 20 km.

The following series of numerical experiments was performed on clouds of 1.75-km radius. The initial cloud droplet spectrum is assumed to be characteristically temperate-continental in structure. Thus, the initial cloud droplet concentration is 300 cm^{-3} with a radius dispersion of 0.25. The natural ice crystal nucleation spectrum is

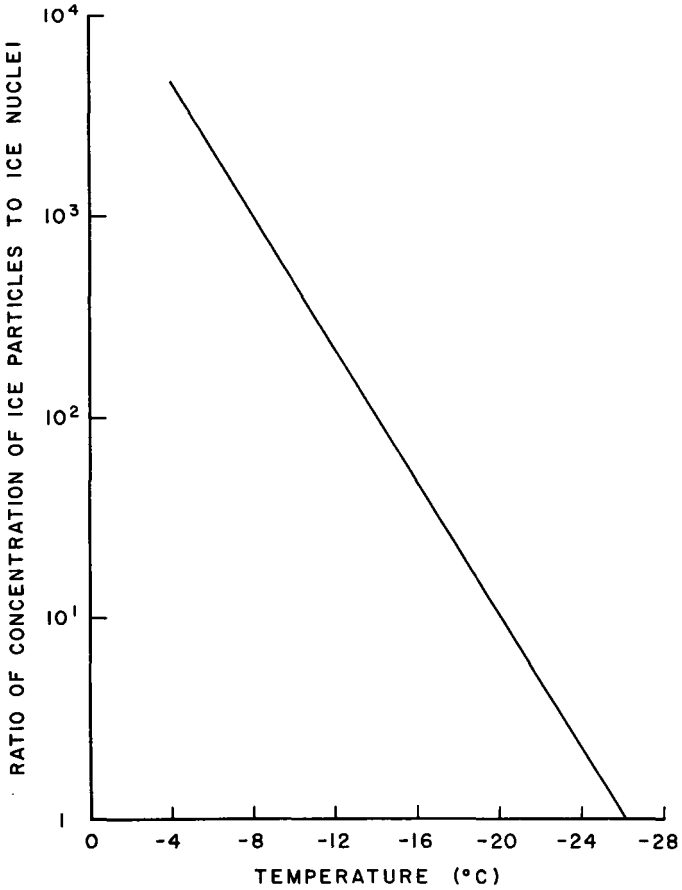

FIGURE 4.—Ratio of the concentration of ice particles to ice nuclei as a function of temperature (Hobbs 1969).

simulated by two models. The first is the exponential model given by eq (77). This model is taken to represent the lower extreme of ice crystal cumulative concentrations. Because it was found in earlier numerical experiments (Lavoié et al. 1970) that the above natural model gave ridiculously low precipitation rates in simulated lake-induced cumuli, another natural model had to be formulated. For a more active natural ice crystal model, eq (77) is multiplied by the ratio of observed ice crystals to ice nuclei as found by Hobbs (1969) and shown in figure 4. The cumulative concentrations of natural ice crystals for the lower bound, a, and the upper bound, a′, are shown in figure 5. Because the exact nature of the pyrotechnic flare employed in this field experiment is unknown to the author, the Olin 1055[1] pyrotechnic activity curve discussed by Simpson et al. (1970) is used to specify the effectiveness of the AgI seeding material. If it is assumed that three 18-g AgI pyrotechnics introduced into the cloud by Davis et al. (1967) burn through a depth of 3 km and the seeding material rapidly becomes mixed across the width of the cloud, the estimated concentration of AgI is 1.8×10^{-12} g/l. Curve b in figure 5 illustrates the corresponding cumulative concentration of crystals activated in the cloud.

Because Davis et al. (1967) observed the cloudbase updraft radius and not the cloud-*tower* radius, these cal-

[1] Mention of a commercial product does not constitute an endorsement.

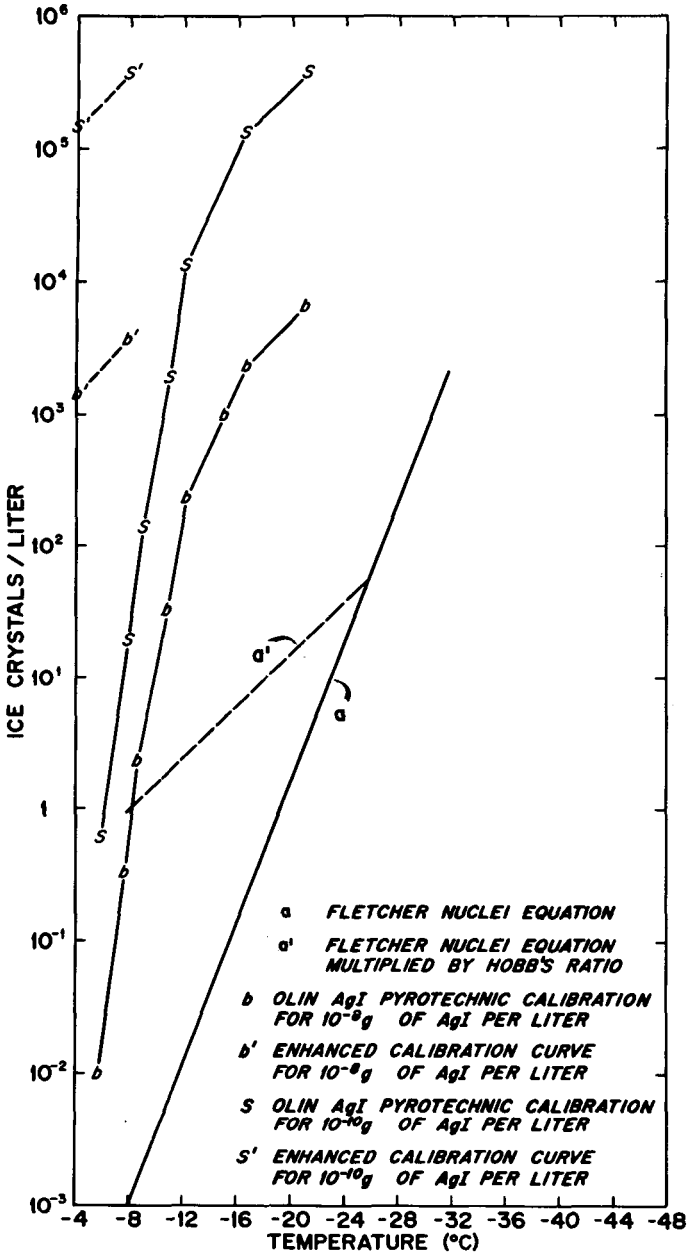

FIGURE 5.—Prescribed nucleated cumulative ice crystal concentration as a function of cloud temperature for natural clouds, a and a′, simulated pyrotechnic seeding, b and s, and enhanced pyrotechnic seeding, b′ and s′.

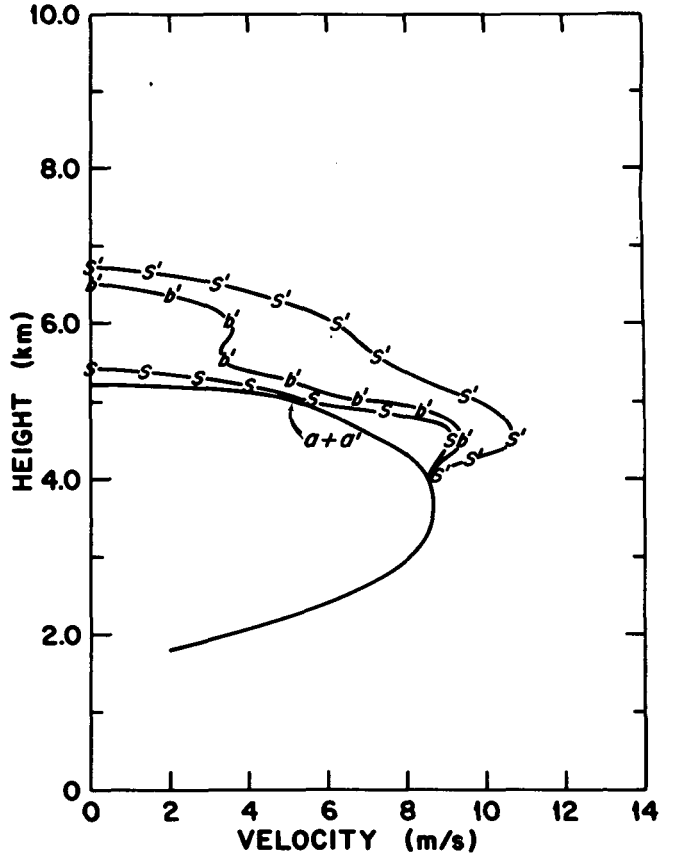

FIGURE 6.—Predicted cloud vertical velocity as a function of height for May 19, 1965, PSU case study (Davis et al. 1967).

culations were performed with the steady-state version of the model. Model predictions of cloud updraft velocity as a function of height are illustrated in figure 6. The predicted cloudtop height of natural clouds a and a′ is 5.2 km, which is in agreement with the observation by Davis et al. (1967) that cloudtops in the area extended from 4.75 to 5.5 km. Seeding the cloud with AgI concentration (curve b) produced no significant alteration in the cloud structure or cloudtop height.

Because Davis et al. (1967) observed the seeded cloud to grow to an altitude of about 9.15 km, we must now determine why the model does not respond to the concentration of crystals specified by curve b in figure 5. To do this, we will first increase the concentration of AgI by approximately two orders of magnitude to 10^{-10} g/l. This concentration corresponds to that amount of AgI generally introduced in south Florida cumuli by Simpson et al. (1970) to induce dynamic development. As illustrated by curve s in figure 6, the model still does not predict extensive vertical development. The fact that neither AgI concentration s nor b resulted in a predicted significant growth may be a consequence of the fact that extensive glaciation either did not occur at all or occurred much too high in the cloud. Figure 7 illustrates that the predicted buoyancy alteration with AgI concentration s was above 5.0 km, which is well within the inversion shown in the sounding in figure 8.

It is apparent that, to predict significant dynamic response, we must somehow force the model to glaciate at much warmer temperatures. The laboratory observations by Steele and Davis (1969) and field observations by Weinstein and Takeuchi (1970) suggest that AgI generator calibrations may be in error by three orders of magnitude at warm temperatures. Let us then suppose that some physical mechanism such as ice crystal multiplication or contact nucleation has enhanced ice crystal production at warm temperatures. To do this, we activate the entire cumulative concentration of crystals formed in the laboratory with AgI concentration s over the temperature range −4° to −8°C as illustrated by curve s′ in figure 5. Furthermore, curve b′ represents a similar modification to curve b.

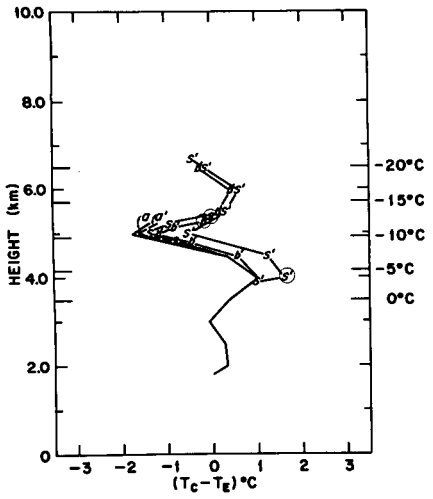

FIGURE 7.—Predicted cloud temperature excess as a function of height for May 19, 1965, PSU case study.

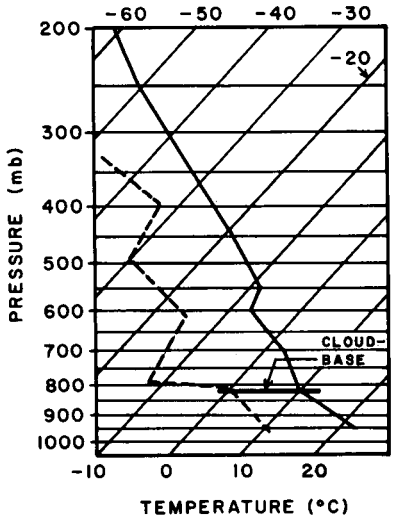

FIGURE 8.—Upper air sounding for May 19, 1965 (Davis et al. 1967).

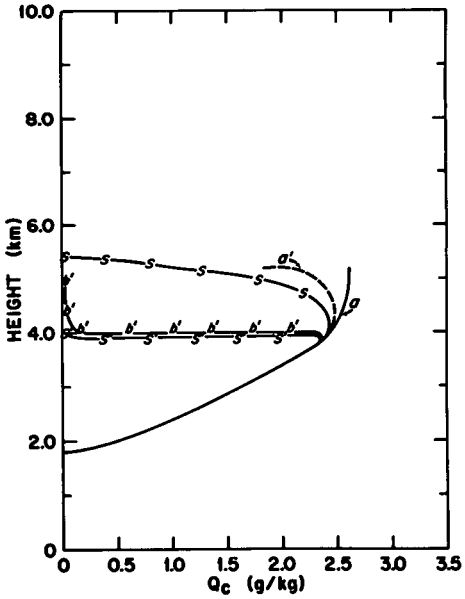

FIGURE 9.—Predicted Q_c as a function of height for May 19, 1965, PSU case study.

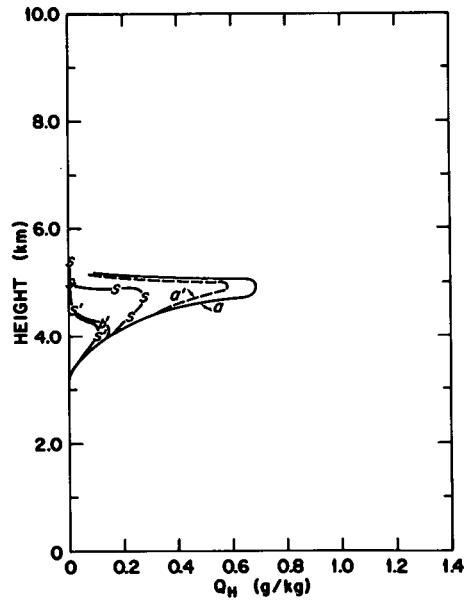

FIGURE 10.—Same as figure 9 for Q_H.

Figure 6 illustrates the predicted cloud vertical velocity profile when seeded with crystal concentrations s′ and b′. In both cases the model predicted an increased cloudtop height of over 1 km.

Figure 7 illustrates that the vertical growth in both experiments s′ and b′ is a consequence of additional heating at temperatures higher than −5°C. Figures 9–12 illustrate the redistribution of water substance that occurred as a consequence of simulated seeding. An important feature in figures 9–12 is the circumstance that when ice crystal production was simulated to occur high in the cloud, such as in natural cloud a′ or seeding experiments s, the water content of frozen material was predicted to be principally in the form of frozen raindrops, Q_F. On the other hand, seeding experiments s′ and b′ transferred most of the water substance to ice crystals, Q_I. This is a consequence of the fact that, in the latter experiments, the crystals were introduced below the level of maximum production of supercooled rainwater, Q_H.

It should be pointed out that although the "seedability" predicted with seeding experiments s′ and b′ is significant, the predicted maximum cloudtop height fell short of the 9.15-km height of the cloud observed by Davis et al. (1967). Since the cloud was also observed to grow laterally to a diameter of 20 km, however, the extent of vertical growth could well have been a consequence of nonlinear dynamic behavior not simulated in this simple model.

Before we make any further conclusions, let us look at the second case study. The second case study chosen for numerical simulation was the one of May 27, 1968, discussed by Simpson and Wiggert (1971). Two clouds of approximately 1.0-km radius were observed on that day. The first cloud was not seeded and was observed to grow to 9.1-km height; the second cloud was seeded with approximately 1 kg of AgI in pyrotechnic form and was observed to grow to about 11.0 km. Because only the cloud-tower radius was observed, these experiments will

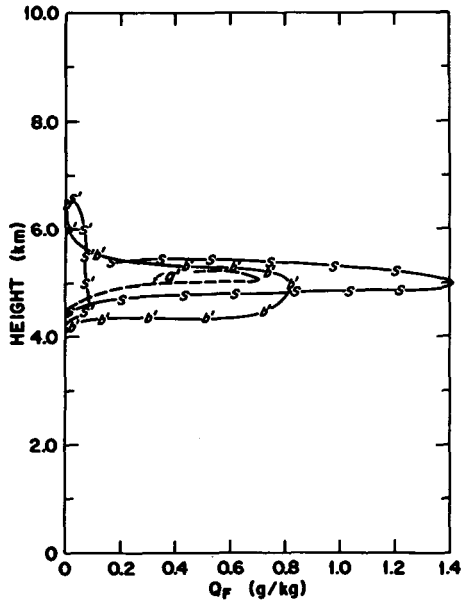

FIGURE 11.—Same as figure 9 for Q_F.

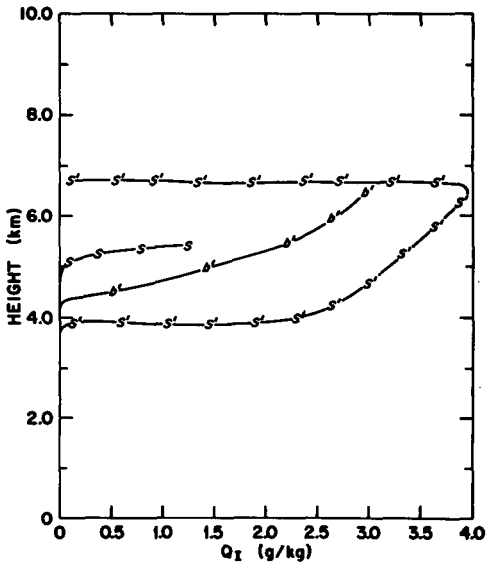

FIGURE 12.—Same as figure 9 for Q_I.

be performed with the EML spherical vortex version of the model.

As in the previous experiments, natural ice crystal production is simulated by curves a and a′ in figure 5. Silver iodide seeding is simulated by curve s in figure 5, which is derived from the AgI activity curve discussed earlier and an estimated 1-kg seeded amount of AgI. The AgI material is assumed to be well mixed across the radius of the cloud and through a depth of 3.0 km. Curve s′ of figure 5 is again assumed to simulate enhanced activity of the AgI aerosol in natural clouds.

Figure 13 illustrates the predicted vertical velocity profiles for "natural" crystal models a and a′ as well as simulated seeding experiments s and s′. An important feature here is that the predicted cloudtops of natural clouds a and a′ exceed the observed top of cloud 12 by 0.5–1.0 km. This overprediction may, in part, be a con-

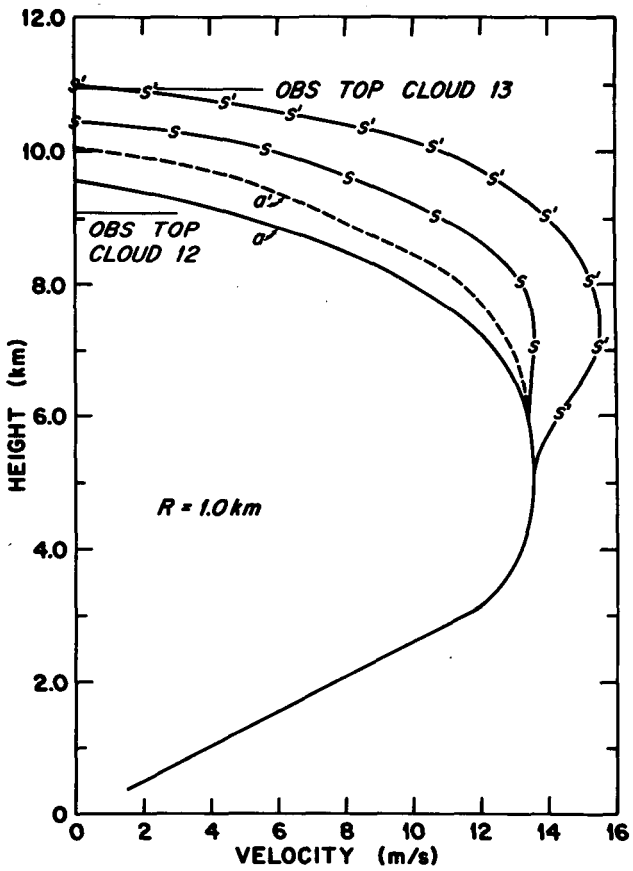

FIGURE 13.—Predicted cloud vertical velocity as a function of height for May 27, 1968, EML case study.

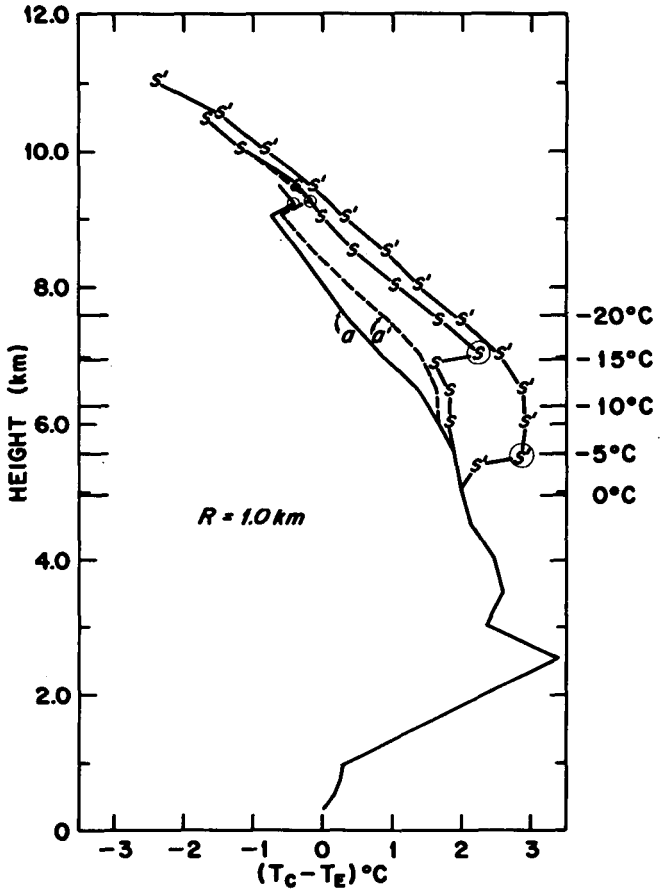

FIGURE 14.—Predicted cloud temperature excess as a function of height for May 27, 1968, EML case study.

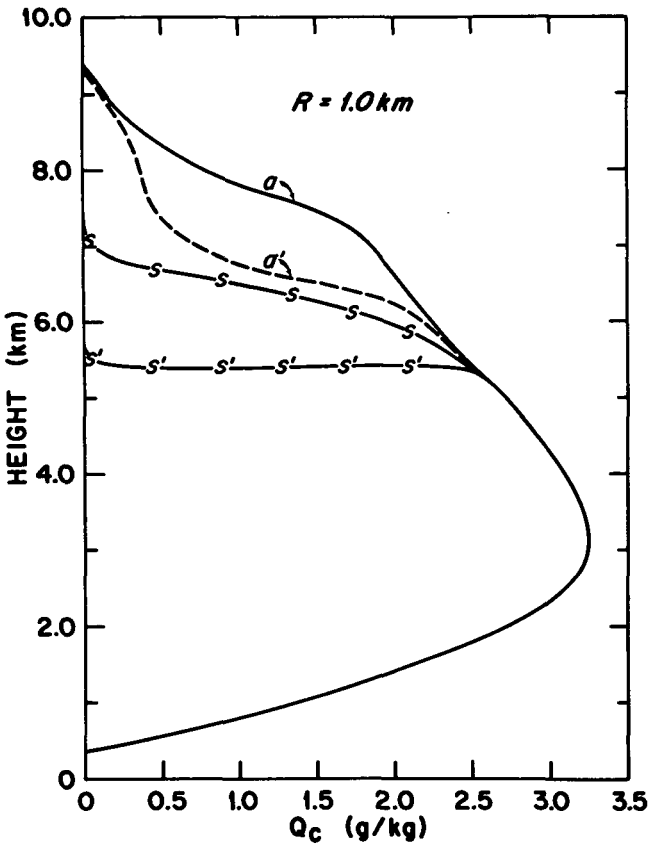

FIGURE 15.—Predicted Q_c as a function of height for May 27, 1968' EML case study.

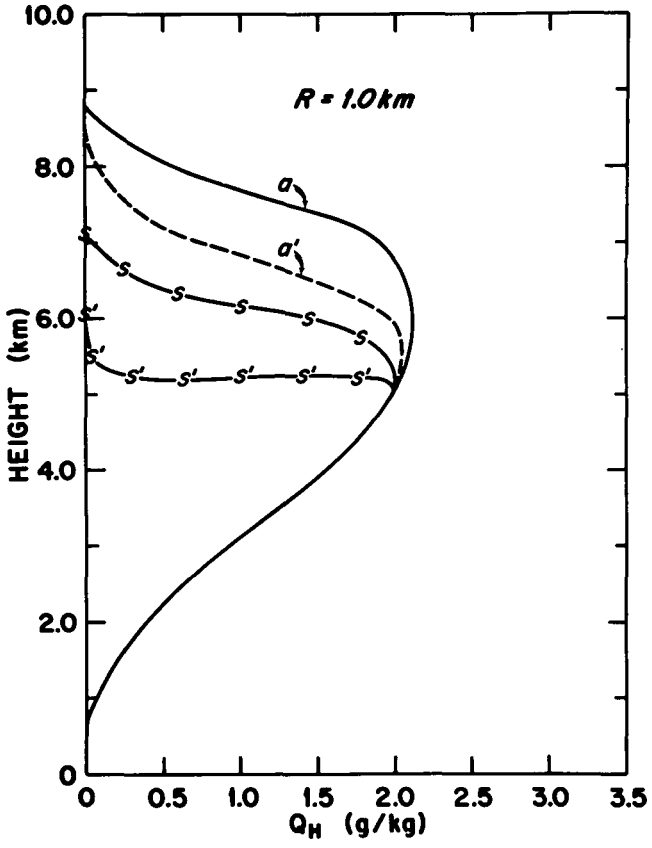

FIGURE 16.—Same as figure 15 for Q_H.

sequence of the predicted glaciation of the cloud at the level of the observed top of cloud 12. As illustrated in figure 14, this resulted in a predicted kink in the temperature-excess curve at the glaciation level. Similar kinks in the temperature-excess curves occur at 7.0 and 5.5 km for seeding experiments s and s′, respectively. This thermodynamic discontinuity is a consequence of the assumption that the cloud immediately relaxes to ice saturation once the cloud water content becomes negligible. Earlier calculations described by Cotton (1970) did not assume this immediate transition. Instead, the cloud mixing ratio was evaluated from the depletion of vapor calculated by the ice crystal model. Unfortunately, the model thermodynamically overshot during this period of transition and led to an even larger discontinuity. To some extent, this local rise in temperature excess is real, but it certainly is spatially too large. It is important to recognize that this approximation may lead to an error in cloudtop height, particularly if glaciation occurs at the level at which the cloud is nearly terminating.

A second important point is that natural crystal model a′ resulted in a predicted cloudtop height 500 m higher than that for natural crystal model a. This is in contrast to the previous case study in which the model did not respond to the higher crystal concentration a′. The source of the model's additional sensitivity to moderate increases in ice crystal concentration may be seen in the calculated profiles of condensed water substance illustrated in figures 15–18. Figures 15 and 16 illustrate quite graphically that the modeled cloud in the EML case study is considerably wetter than the clouds observed in the Pennsylvania State University (PSU) case study. As a consequence, the EML case study has a much larger amount of supercooled water available for fusion than the PSU case study. Furthermore, because of the larger amount of total condensed water, the EML case study has a proportionately larger amount of Q_H. Given this proportionately larger amount of Q_H, a moderate increase in crystal concentration (i.e., to a′) will lead to a significant release of latent heat of fusion through the mechanism of raindrop freezing by collection of ice crystals.

Seeding the cloud with AgI concentration s led to a predicted cloudtop height 400 m above that of natural cloud a′. In comparison with the PSU case study, this growth is significant. However, as shown in figure 13, the predicted height is well below the observed height of cloud 12. Numerical experiments with enhanced AgI activity (curve s′) resulted in a predicted cloudtop height that is in excellent agreement with the observed height of cloud 12. Figures 17 and 18 illustrate a major distinction between simulated seeding experiments s and s′. In the former experiment, glaciation occurred principally by the formation of Q_F, whereas in the latter experiment it occurred principally by the formation of Q_I. This illustrates that seeding experiment s′ resulted in a major alteration of the colloidal structure of the cloud, whereas experiment s produced a colloidal structure that was qualitatively similar to the natural cloud model a′.

Looking at the PSU and EML case studies together, we see that in neither case did the cloud dynamically respond

478-887 O - 72 - 4

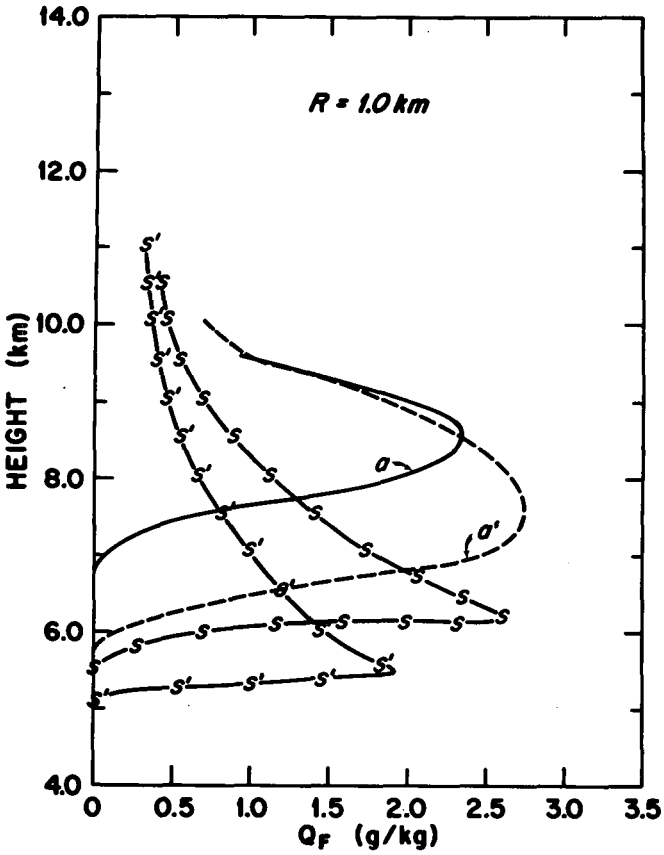

FIGURE 17.—Same as figure 15 for Q_F.

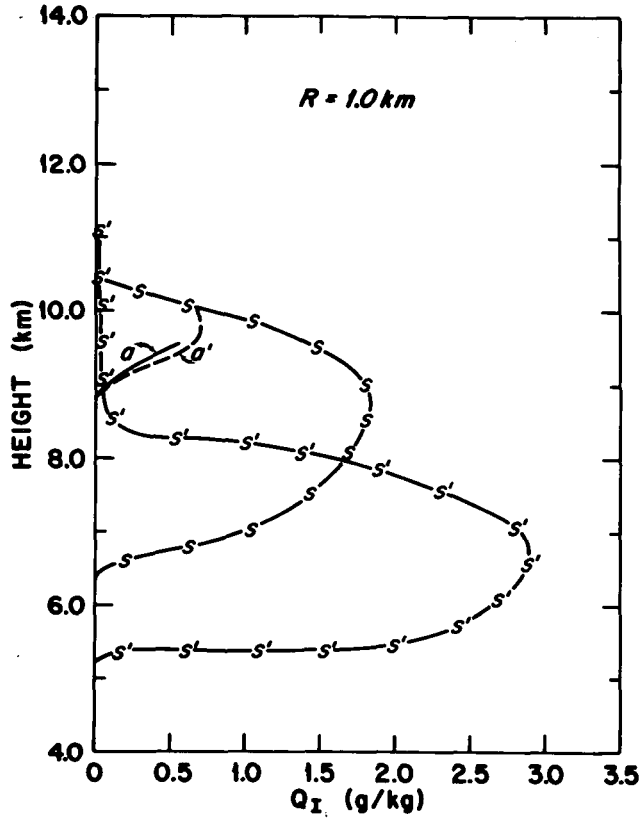

FIGURE 18.—Same as figure 15 for Q_I.

significantly to the estimated concentration of crystals formed by actual AgI pyrotechnic calibrations. This leads one to suspect that the calibrations are in error and that the enhanced calibration curves b′ and s′ are perhaps more representative of the actual production of crystals in the cloud. It would, however, be foolish to conclude at this time that these results confirm our suspicions that ice crystal production is far more efficient than our laboratory simulators suggest. Additional sources of uncertainty in the model, such as (1) the growth rate of individual ice particles, (2) the rate of production of Q_H, or (3) the vertical velocity field, could lead to similar discrepancies.

Certainly, the net growth predictions of ice particles could be in error (in time) by as much as 30 to 50 percent. This could not, however, account for the two–three order-of-magnitude increase in crystal concentrations at high temperatures represented by experiments b′ and s′.

As far as the rate of production of Q_H is concerned, Cotton (1972) demonstrated that his parameterization of the collection process is an extremely good simulation of Berry's numerical collection experiments. Furthermore, numerical experiments with the formulation in a one-dimensional, time-dependent model discussed by Cotton (1971) demonstrated that the technique resulted in rainwater fields that were in good agreement with observations.

The remaining uncertainty in the model, namely, the vertical velocity field, cannot be considered a negligible source of error. Neither the steady-state nor the spherical vortex models can predict the magnitude of vertical motion within 30 percent of actual cloud values. Sensitivity experiments have demonstrated that a 30-percent decrease in cloud vertical velocity can lead to alterations in cloudtop height as large as a two–three order-of-magnitude increase in crystal concentration at high temperatures. This occurs because the reduced vertical velocity results in increased time for ice particle growth, which leads to proportionately more latent heat of fusion at a given level. We are thus led to conclude that, although the model responded well to the enhanced pyrotechnic calibrations s′ and b′, we cannot rule out the possibility that uncertainties in cloud vertical velocities could well account for a similar model response.

11. SENSITIVITY TO PRECIPITATION FALLOUT

It is well known that in models of nonsupercooled cumuli the addition of a precipitation process will lead to lower total water contents high in the cloud and subsequently larger effective bouyancy. This, in turn, results in a predicted cloudtop height that is often higher in a precipitating cloud than in a nonprecipitating cloud.

In the case of a supercooled cumulus model, however, the presence of a warm-cloud precipitation mechanism leads to several peculiar interactions. In the first place, it has been shown that, for a given concentration of ice particles, the presence of supercooled precipitation will lead to rapid glaciation of the cloud by the process of

raindrop collection of ice particles. Thus, the presence of a warm-cloud precipitation process will increase the rate of release of the latent heat of fusion and often result in a predicted cloudtop that is higher than in a nonprecipitating cloud. We have, however, already pointed out that the addition of a warm-cloud precipitation process leads to lower total water contents high in the cloud. It can easily be shown that the bouyancy gain due to the latent heat of fusion of condensed water is greater than the bouyancy loss due to the weight of the same amount of water. Thus, given that a cloud may penetrate deep into a supercooled layer, the presence of a warm-cloud precipitation mechanism could result in a reduction in predicted cloudtop height simply due to the loss of potential energy in the form of total supercooled water. In terms of the dynamic behavior of the cloud, it would appear that the most efficient cloud would be one that does not form precipitation by warm-cloud mechanisms until it penetrates deep into a supercooled region where the presence of large amounts of total supercooled water in the form of precipitation will result in the rapid release of the latent heat of fusion. The possible implications of this conclusion on the dynamic behavior of supercooled cumuli in polluted air masses are many.

12. SUMMARY AND CONCLUSIONS

A numerical model has been developed to explore the processes of cumulus cloud glaciation and the consequences of the latent heat so released. Two case studies have been analyzed. In neither case study did the simulated seeded clouds grow to observed cloudtop heights when crystal concentrations were estimated from AgI pyrotechnic calibrations. When the crystal concentrations were increased by 2–3 orders of magnitude at warm temperatures, however, the model responded by predicting significant increases in cloudtop height. This response could be interpreted as further evidence that laboratory simulators of ice crystal production do not simulate all the processes in real clouds. It was pointed out, though, that 30-percent errors in predicted vertical velocity could lead to similar cloud responses in some soundings.

The results of the two case-study experiments illustrated that the principle action of ice particles nucleated on sublimation nuclei or by the freezing of cloud droplets in cumulus clouds containing moderate to heavy amounts of supercooled rainwater is to promote the freezing of supercooled rainwater. On the other hand, clouds containing small amounts of supercooled rainwater are dynamically insensitive to moderate concentrations of ice crystals. In such clouds, extensive riming and vapor-deposition growth of crystals in concentrations of several thousand per liter are required before they make significant contributions to the dynamic structure of the cloud. Finally, it was found that the warm-cloud precipitation process can either invigorate or retard the dynamic behavior of a supercooled cloud, depending upon the height and magnitude of the precipitation process.

ACKNOWLEDGMENTS

I would like to express my appreciation to Ronald Lavoie of the Department of Meteorology, The Pennsylvania State University, for his many suggestions and stimulating discussions throughout the study. I am also grateful to Joanne Simpson for her support in the final preparation of the manuscript. Robert N. Powell prepared many of the figures and Peggy M. Lewis typed the manuscript. This work was carried out in part as a Ph. D. dissertation study at The Pennsylvania State University under Grants NSF–GA–777, NSF–GA–3956, and NSF–GA–13818 from the National Science Foundation and Contract No. E22–103–68(N) from ESSA (now NOAA), Atmospheric Physics and Chemistry Laboratory.

REFERENCES

Bashkirrova, G. M., and Pershina, T. A., "O masse snezhinok i skorosti ikh padeniia" (Mass of Snowflakes and Their Speed of Fall), *Trudy Glavnaia Geofizicheskaia Observatoriia* No. 156, Leningrad, U.S.S.R., **1964**, pp. 83–100.

Byers, Horace Robert, *Elements of Cloud Physics*, University of Chicago Press, Ill., **1965**, 191 pp. (see pp. 109–127).

Cotton, William R., "A Numerical Simulation of Precipitation Development in Supercooled Cumuli," *Report* No. 17, NSF Contract No. NSF GA–13818, Department of Meteorology, The Pennsylvania State University, University Park, Nov. **1970**, 178 pp.

Cotton, William R., "A Comparison of Predicted Precipitation Amounts for Several Warm Cloud Autoconversion Formulations," *Proceedings of the International Conference on Weather Modification, Canberra, Australia, September 6–11, 1971*, American Meteorological Society, Boston, Mass., **1971**, pp. 175–178.

Cotton, William R., "Numerical Simulation of Precipitation Development in Supercooled Cumuli: Part I," *Monthly Weather Review*, Vol. 100, No. 11, Nov. **1972**, pp. 757–763.

Davies, C. N., and Peetz, C. V., "Impingement of Particles on a Transverse Cylinder," *Proceedings of the Royal Society of London*, Ser. A, Vol. 234, No. 1197, England, Feb. **1956**, p. 269.

Davis, Larry G., Kelley, Jean I., and Mack, Eugene J., "An Investigation of the Dynamics and Microphysics of Clouds," *NSF Report* No. 10 (*Final Report*), NSF Grant No. GP–4743, Department of Meteorology, The Pennsylvania State University, University Park, June **1967**, 201 pp.

de Pena, R. G., Iribarne, J. V., and de Achával, E. M., "The Freezing of Supercooled Droplets of Electrolytic Solutions," *Journal of the Atmospheric Sciences*, Vol. 19, No. 4, July **1962**, pp. 302–308.

Fletcher, Neville Horner, *The Physics of Rainclouds*, Cambridge University Press, England, **1962**, 386 pp.

Fuchs, N. A., *The Mechanics of Aerosols*, Pergamon Press, New York, N.Y., **1964**, 408 pp.

Gradshteyn, I. S., and Ryzhik, I. M., *Table of Integrals, Series and Products*, Academic Press, New York, N.Y., **1965**, 1083 pp.

Hallett, J., and Mason, B. J., "The Influence of Temperature and Supersaturation on the Habit of Snow Crystals From the Vapor," *Proceedings of the Royal Society of London*, Ser. A, Vol. 247, No. 1251, England, Oct. **1958**, pp. 440–453.

Hobbs, Peter V., "Ice Multiplication in Clouds," *Journal of the Atmospheric Sciences*, Vol. 26, No. 2, Mar. **1969**, pp. 315–318.

Howell, Wallace E., and Lopez, Manuel, "Project Rainstart," *Interim Report*, Contract No. NSF–C453, E. Bollay Associates, Inc., Boulder, Colo., **1968**, 66 pp.

Jones, R. F., "Size-Distribution of Ice Crystals in Cumulonimbus Clouds," *Quarterly Journal of the Royal Meteorological Society*, Vol. 86, No. 368, London, England, Apr. **1960**, pp. 187–194.

Kessler, Edwin, "On the Continuity of Water Substance," *ESSA Technical Memorandum* IERTM–NSSL 33, U.S. Department of Commerce, National Severe Storms Laboratory, Norman Okla., Apr. **1967**, 125 pp.

Kobayashi, Teisaku, "Experimental Researches on the Snow Crystal Habit and Growth by Means of a Diffusion Cloud Chamber," *Journal of the Meteorological Society of Japan*, 75th Anniversary Volume, Tokyo, Nov. **1957**, pp. 38–47.

Kobayashi, Teisaku, "Experimental Researches on the Snow Crystal Habit and Growth Using a Convection-Mixing Chamber," *Journal of the Meteorological Society of Japan*, Ser. 2, Vol. 38, No. 5, Tokyo, Oct. **1960**, pp. 231–238.

Langham, E. J., and Mason, B. J., "The Heterogeneous and Homogeneous Nucleation of Supercooled Water," *Proceedings of the Royal Society of London*, Ser. A, Vol. 247, No. 125, England, Oct. **1958**, pp. 493–504.

Langmuir, Irving, and Blodgett, Katharine B., *A Mathematical Investigation of Water Droplet Trajectories*, General Electric Co., Schenectady, N.Y., July **1945**, 47 pp.

Lavoie, R. L., Cotton, W. R., and Hovermale, J. B., "Investigations of Lake-Effect Storms," *Final Report*, Contract No. E22–103–68(N), Department of Meteorology, The Pennsylvania State University, University Park, Jan. **1970**, 127 pp.

Liu, J. Y., and Orville, Harry D., "Numerical Modeling of Precipitation Effects on a Cumulus Cloud," *Technical Report* 68–9, Contract No. 14–06–D–5979, South Dakota School of Mines and Technology, Rapid City, Aug. **1968**, 70 pp.

Macklin, W. C., "The Density and Structure of Ice Formed by Accretion," *Quarterly Journal of the Royal Meteorological Society*, Vol. 88, No. 375, London, England, Jan. **1962**, pp. 30–50.

Macklin, W. C., and Ludlam, F. H., "The Fallspeeds of Hailstones," *Quarterly Journal of the Royal Meteorological Society*, Vol. 87, No. 371, London, England, Jan. **1961**, pp. 72–81.

Magono, Choji, "On the Falling Velocity of Solid Precipitation Elements," *Science Reports*, Sec. 1, No. 3, National University, Yokohama, Japan, Mar. **1954**, pp. 33–40.

Magono, Choji, and Lee, Chung Woo, "Meteorological Classification of Natural Snow Crystals," *Journal of the Faculty of Science, Geophysics*, Ser. 7, Vol. 2, No. 4, Hokkaido University, Japan, Nov. **1966**, pp. 321–335.

Marshall, J. S., and Palmer, W. McK., "The Distribution of Raindrops With Size," *Journal of Meteorology*, Vol. 5, No. 4, Aug. **1948**, pp. 165–166.

Murray, F. W., "Numerical Models of a Tropical Cumulus Cloud With Bilateral and Axial Symmetry," *Monthly Weather Review*, Vol. 98, No. 1, Jan. **1970**, pp. 14–28.

Nakaya, Ukichiro, *Snow Crystals: Natural and Artificial*, Harvard University Press, Cambridge, Mass., **1954**, 510 pp.

Ono, A., "The Shape and Riming Properties of Ice Crystals in Natural Clouds," *Journal of the Atmospheric Sciences*, Vol. 26, No. 1, Jan. **1959**, pp. 138–147.

Ono, A., "Growth Mode of Ice Crystals in Natural Clouds," *Journal of the Atmospheric Sciences*, Vol. 27, No. 4, July **1970**, pp. 649–658.

Podzimek, J., "Aerodynamic Conditions of Ice Crystal Aggregation," *Proceedings of the International Conference on Cloud Physics, Toronto, Canada, August 26–30, 1968*, American Meteorological Society, Boston, Mass., **1968**, pp. 296–299.

Ranz, W. E., and Wong, J. B., "Impaction of Dust and Smoke Particles on Surface and Body Collectors," *Industrial and Chemical Engineering*, Vol. 44, No. 6, American Chemical Society, Washington, D.C., June **1952**, pp. 1371–1381.

Schaefer, Vincent J., "New Field Evidence of Inadvertent Modification of the Atmosphere," *Proceedings of the First National Conference on Weather Modification, Albany, New York, April 28–May 1, 1968*, American Meteorological Society, Boston, Mass., **1968**, pp. 163–172.

Shishkin, N. S., "On Snow Crystal Growth in Clouds," *Proceedings Supplement, International Conference on Cloud Physics, Tokyo and Sapporo, Japan, May 22–June 1, 1965*, Oct. **1965**, pp. 136–146.

Simpson, Joanne, and Wiggert, Victor, "Models of Precipitating Cumulus Towers," *Monthly Weather Review*, Vol. 97, No. 7, July **1969**, pp. 471–489.

Simpson, Joanne, and Wiggert, Victor, "1968 Florida Seeding Experiment: Numerical Model Results," *Monthly Weather Review*, Vol. 99, No. 2, Feb. **1971**, pp. 87–118.

Simpson, Joanne, Woodley, William L, Friedman, Howard A., Slusher, Thomas W., Scheffee, R. S., and Steele, Roger L., "An Airborne Pyrotechnic Cloud Seeding System and Its Use," *Journal of Applied Meteorology*, Vol. 9, No. 1, Feb. **1970**, pp. 109–122.

Squires, P., and Turner, J. S., "An Entraining Jet Model for Cumulo-Nimbus Updraughts," *Tellus*, Vol. 14, No. 4, Stockholm, Sweden, Nov. **1962**, pp. 422–434.

Steele, Roger L., and Davis, C. I., "Variation of Ice Nuclei Effectiveness With Liquid Water," *Journal of the Atmospheric Sciences*, Vol. 26, No. 2, Mar. **1969**, pp. 329–330.

Stommel, Henry, "Entrainment of Air Into a Cumulus Cloud," *Journal of Meteorology*, Vol. 4, No. 3, June **1947**, pp. 91–94.

Todd, Clement J., *A System for Computing Ice-Phase Hydrometeor Development*, Arg 64 Pa–121, Atmospheric Research Group, Meteorological Research, Inc., Altadena, Calif., **1964**, 30 pp.

Vali, Gabor, and Stansbury, E. J., "Time-Dependent Characteristics of the Heterogeneous Nucleation of Ice," *Canadian Journal of Physics*, Vol. 44, No. 3, Ottawa, Mar. **1966**, pp. 477–502.

Weickmann, H. K., Katz, U., and Steele, R., "AgI-Sublimation or Contact Nucleus?," *Preprints of papers presented at the Second Conference on Weather Modification, Santa Barbara, California, April 6–9, 1970*, American Meteorological Society, Boston, Mass., **1970**, pp. 332–336.

Weinstein, Allen Ira, and Davis, Larry G., "A Parameterized Numerical Model of Cumulus Convection," *Report* 11, NSF Grant GA–777, Department of Meteorology, The Pennsylvania State University, University Park, May **1968**, 43 pp.

Weinstein, Allen Ira, and Takeuchi, D. M., "Observations of Ice Crystals in a Cumulus Cloud Seeded by Vertical-Fall Pyrotechnics," *Journal of Applied Meteorology*, Vol. 9, No. 2, Apr. **1970**, pp. 265–268.

[*Received March 15, 1971; revised March 8, 1972*]